

**TIMING OF LATE HOLOCENE PALEOEARTHQUAKES ON THE NORTHERN SAN  
ANDREAS FAULT AT THE FORT ROSS ORCHARD SITE,  
SONOMA COUNTY, CALIFORNIA**

Keith I. Kelson, Ashley R. Streig<sup>1</sup>, and Richard D. Koehler<sup>2</sup>  
William Lettis & Associates, Inc.  
1777 Botelho Dr., Suite 262, Walnut Creek, CA 94596  
Phone: (925) 256-6070; Fax: (925) 256-6076  
kelson@lettis.com

Submitted to  
U.S. Geological Survey  
National Earthquake Hazard Reduction Program

June 2005

This research was supported by the U.S. Geological Survey (USGS), Department of the Interior, under USGS award numbers 01-HQ-GR-0072 and 02-HQ-GR-0069. The views and conclusions contained in this document are those of the authors and should not be interpreted as necessarily representing the official policies, either expressed or implied, of the U.S. Government.

---

<sup>1</sup> Present address: Taipei, Taiwan; ashleystreig@hotmail.com

<sup>2</sup> Present address: Center for Neotectonic Studies, University of Nevada, Reno, NV; koehler@seismo.unr.edu

**AWARD NO. 02HQGR0069**

**TIMING OF LATE HOLOCENE PALEOEARTHQUAKES ON THE NORTHERN SAN  
ANDREAS FAULT AT THE FORT ROSS ORCHARD SITE, SONOMA COUNTY,  
CALIFORNIA**

Keith I. Kelson, Ashley R. Streig, and Richard D. Koehler  
William Lettis & Associates, Inc.  
1777 Botelho Dr., Suite 262, Walnut Creek, CA 94596  
Phone: (925) 256-6070; Fax (925) 256-6076  
kelson@lettis.com

**ABSTRACT**

---

Paleoseismic trenching within Fort Ross State Historic Park provides data on the late Holocene rupture history of the North Coast segment of the northern San Andreas fault. The 1906 earthquake ruptured through the Fort Ross Orchard site, which is characterized by a narrow shutter ridge and associated linear trough containing latest Holocene sediments. Trenches across the northeast-facing fault scarp exposed scarp-derived colluvial deposits, possible fissure-fill deposits, and tentative upward fault truncations that provide evidence of three possible surface ruptures prior to 1906. Coarse-grained scarp-derived colluvial sediments were deposited after individual surface-rupturing earthquakes pre-date the 1906 rupture and constrain the timing of earthquakes over the past approximately 1100 years. Based on stratigraphic ordering and a statistical comparison of radiocarbon dates using the OxCal program, we estimate (at a 95% confidence level) that the past four surface ruptures at the Orchard site occurred at AD 1906, AD 1630 to 1776, AD 1210 to 1380, and AD 300 to 1050. Our re-analysis of stratigraphic relationships and radiocarbon ages of the nearby Fort Ross Archae Camp site are consistent with these dates, and further constrain the earliest of this series to have occurred between AD 920 and 1050. The time windows for these ruptures are consistent with results from other sites on the North Coast segment of the fault.

## TABLE OF CONTENTS

---

ABSTRACT.....	i
1.0 INTRODUCTION .....	1
2.0 GEOLOGIC SETTING OF THE FORT ROSS ORCHARD SITE.....	2
3.0 PALEOSEISMIC RESULTS.....	4
3.1 Stratigraphy and Structure of Trench 1 .....	4
3.2 Stratigraphy and Structure of Trenches 4 and 5 .....	5
3.3 Deposit Age Estimates .....	8
4.0 NUMBER AND TIMING OF SURFACE-RUPTURING EARTHQUAKES.....	10
5.0 COMPARISON WITH PUBLISHED NORTH COAST RUPTURE CHRONOLOGIES .....	12
6.0 CONCLUSIONS.....	15
7.0 ACKNOWLEDGEMENTS .....	16
8.0 REFERENCES .....	17

## LIST OF TABLES

---

Table 1. Summary of Radiocarbon Analyses, Fort Ross Orchard Site.....	9
Table 2. Age estimates for four most-recent surface-rupturing earthquakes on the North Coast section of the San Andreas fault at the Fort Ross Orchard site. Age ranges represent uncertainty levels estimated by the OxCal analytical program (Ramsey, 2003).....	11
Table 3. Summary of age estimates for recent surface-rupturing earthquakes on the San Andreas fault at the Archae Camp and Fort Ross Orchard sites. Age ranges represent uncertainty levels estimated by the OxCal analytical program (Ramsey, 2003). .....	13

## LIST OF FIGURES

---

- Figure 1. Regional map of major faults in northwestern California, showing San Andreas fault segments from WGCEP (2003), previous paleoseismic sites, and the distribution of surface and geodetic slip produced by the 1906 rupture (Thatcher et al., 1997).
- Figure 2. Topographic map of the Fort Ross area, showing locations of recent paleoseismic sites on the San Andreas fault and documented offsets from the 1906 earthquake.
- Figure 3. Photograph of trenches 4 and 5 at the Fort Ross Orchard site, looking southwest across the San Andreas fault.

- Figure 4. Detailed topographic map of the Fort Ross Orchard site, showing San Andreas fault, and trenches T1 to T5. Contour interval of 1 m uses arbitrary site datum.
- Figure 5. Logs from trench 1, Fort Ross Orchard site; (A) northwestern wall, (B) southeastern wall.
- Figure 6. Photograph of San Andreas fault exposed in southeastern wall of Trench 1, showing bedrock on southwestern side of fault, faulted colluvium and alluvium on northeastern side of fault, fissure-fill deposits, and unfaulted colluvium deposited since 1906.
- Figure 7. Log of northwestern wall of trench 4, Fort Ross Orchard site.
- Figure 8. Logs of northwestern and southeastern walls of trench 5, Fort Ross Orchard site. See Figure 7 for generalized unit descriptions.
- Figure 9. Stratigraphic relationships on the eastern side of the San Andreas fault, Fort Ross Orchard site.
- Figure 10. Calibrated 2-sigma radiocarbon ages plotted by relative stratigraphic order. Sample number in circles are from trench 1; sample numbers in squares are from trench 5. Samples highlighted in yellow are those interpreted as most representative of deposit age, and are used in OxCal analysis program.
- Figure 11. Analytical output from OxCal v 3.9 (Ramsey, 2003), showing radiocarbon sample numbers within each phase, agreement percentages, and probability density functions of each sample and earthquake events.
- Figure 12. Earthquake chronology along segments of the northern San Andreas fault. Open bars show 1-sigma confidence intervals; solid bars show 2-sigma confidence intervals.

## 1.0 INTRODUCTION

---

Geologic data on the timing of past events are essential for evaluating rupture segmentation of the northern San Andreas fault and for estimating the probabilities and magnitudes of future earthquakes in the San Francisco Bay region (Working Group on California Earthquake Probabilities [WGCEP], 2003). Developing well-constrained chronologies of late Holocene surface ruptures at sites along the northern San Andreas fault is critical for identifying possible fault rupture segments, characterizing relationships among rupture segments during individual earthquakes, and evaluating the complete earthquake cycle in terms of relationships between characteristically long, 1906-type multi-segment ruptures and smaller, shorter ruptures. While studies at individual sites cannot address these regional issues revolving around fault behavior, the basis for understanding long-term fault behavior lies in the assessment of site-specific paleoseismologic information on earthquake timing, amounts of coseismic slip, and fault slip rate. This study is focused on obtaining data on the timing of surface ruptures at a site along the North Coast segment of the northern San Andreas fault (Figure 1), as a contribution to understanding these larger, more regional issues.

The northern San Andreas fault contains four primary segments (WGCEP, 2003), including the Offshore segment from Cape Mendocino to near Point Arena, the North Coast segment from Point Arena to the Golden Gate, the Peninsula segment from the Golden Gate to Los Gatos, and the Santa Cruz Mountains segment from Los Gatos to San Juan Bautista (Figure 1). The great  $M_w$ 7.8 San Francisco earthquake of 1906 produced 470 km of surface rupture between San Juan Bautista and Cape Mendocino (Lawson, 1908; Thatcher et al., 1997; Prentice et al., 1999) (Figure 1), including rupture on all four of these segments. The WGCEP (1999, 2003) considered several alternative rupture models for the northern San Andreas fault, including models in which it ruptures during earthquakes similar in size to the 1906 event or in smaller magnitude ( $M_w \leq 6.9$ ) earthquakes along one, two, or three of these fault segments. The WGCEP (2003) also considered the possibility of a smaller earthquake in the Fort Ross area through inclusion of a floating,  $M_w$ 6.9 earthquake anywhere along the 470-km-long 1906 rupture. These different models have significant implications for the recurrence of various magnitudes of earthquakes, and thus for the probabilities of earthquakes along this section of the fault. The WGCEP (2003) rupture models and weightings reflect a consensus view that the fundamental behavior of the San Andreas fault is expressed as full-length ruptures similar to the 1906 earthquake, with lesser likelihoods of smaller segment ruptures.

Obtaining paleoseismic data on the timing of late Holocene earthquakes on the North Coast segment helps address these possible rupture scenarios. Of primary importance is obtaining information on the timing of the penultimate large earthquake, and on the recurrence of surface ruptures during roughly the past two thousand years. Collectively, several studies (Prentice, 1989; Niemi and Hall, 1992; Noller et al., 1993; Simpson et al., 1996; Baldwin, 1996; Knudsen et al., 2002; Niemi et al., 2002, 2003; Fumal et al., 1999, 2004) support a range in recurrence for large earthquakes on the North Coast segment of the San Andreas fault of 180 to 370 years (WGCEP, 2003). To help reduce this uncertainty in characterizing the northern San Andreas fault, further refinement of the chronology of large surface ruptures along the fault is required. This investigation focuses on obtaining data on the timing of large surface-rupturing earthquakes along the North Coast segment of the San Andreas fault at Fort Ross State Historic Park (Figure 1). This effort contributes important information for characterizing the behavior of the northern San Andreas fault in the San Francisco Bay region.

## 2.0 GEOLOGIC SETTING OF THE FORT ROSS ORCHARD SITE

---

Between Fort Ross and Point Arena, the San Andreas fault forms the boundary between the Gualala structural block on the southwest and the uplifted Coast Ranges on the northeast (Figure 2). Southwest of the Fort Ross Orchard site, the Gualala block is associated with remnants of at least three emergent marine terraces (Prentice, 1989; Muhs et al., 2003), which form a stepped topography between the site and the Pacific coastline (Figure 2). Several steep-walled ravines are incised into the Gualala block, including Kolmer Gulch northwest of the Fort Ross Orchard site, Fort Ross Creek and Mill Gulch southeast of the site, and several tributaries to these streams (Figure 2). Locally, the San Andreas fault lies within northwest-trending sections of these ravines, which have steep valley walls and dense vegetation. The areas between the major incised ravines are characterized by rolling topography that is strongly affected by surface fault deformation and/or landsliding. Previous paleoseismic sites in the Fort Ross area have been located in these moderate-relief interfluvial areas, including the Mill Gulch site (Prentice et al., 2000, 2001) and the Archae Camp site (Noller et al., 1993; Simpson et al., 1996; Noller and Lightfoot, 1997) (Figure 2). The Fort Ross Orchard site is in the interfluvial area between the southern arm of Kolmer Gulch and Fort Ross Creek, about 1.0 km northwest of the Archae Camp site and about 2.8 km northwest of the Mill Gulch site (Figure 2).

In the vicinity of Fort Ross, the fault is associated with prominent geomorphic features, including side-hill benches, sag ponds, linear drainages, shutter ridges, and uphill-facing scarps (Brown and Wolfe, 1972; Prentice, 1989; Figure 2). Matthes (in Lawson, 1908) noted offsets in cultural features as a result of the 1906 rupture, including 2.3 m of offset of Fort Ross Road, 3.6 m of offset of an unnamed ranch road about 250 m southeast of Fort Ross Road, and 3.6 m of offset of a fence about 1.2 km southeast of Fort Ross Road (Figure 2). The offset measured at Fort Ross Road is lower because a secondary fault strand west of the Fort Ross Orchard site probably experienced some coseismic slip. Contemporary photographs show that the 1906 rupture at the Fort Ross Orchard site produced a northeast-facing scarp along the main fault strand (Lawson, 1908; Bancroft Library Archives, from C. Prentice, USGS, personal communication, 2003). This northeast-facing fault scarp is a dominant feature of the present-day topography through the site (Figure 3).

The Fort Ross Orchard site was chosen for investigation because it has (1) excellent geomorphic relations that constrain the location of the main strand of the fault, (2) late Holocene deposits in a linear valley, and (3) minimal cultural disturbance. The site includes a prominent, northwest-trending linear shutter ridge, an uphill-facing scarp, and a linear depression that clearly mark the location of the main strand of the fault (Figure 4). The northeastern side of the narrow, linear shutter ridge forms a 1- to 4-m-high fault scarp that faces uphill relative to the regional slope, and is associated with a linear depression that marks the location of the main strand of the San Andreas fault (Figure 4). In the southeastern part of the orchard, the linear ridge acts as a buttress for alluvial-fan sediment derived from a small, incised drainage gully northeast of the site (Figure 4). These alluvial-fan sediments were exposed in our initial trenches excavated in 2000 (Trenches 1 to 3, Kelson et al., 2003). In contrast, the central part of the Orchard site includes a 30-m-long, 2-m-deep closed depression that contains ponded water most of the year (Figure 4). North of the closed depression and directly northeast of the highest part of the linear ridge crest, the fault borders a linear trough that slopes gently to the northwest. Trenches 4 and 5 were excavated in this northern area in 2004, and exposed a sequence of colluvium shed from the linear ridge and from the colluvial hillslope northeast of the linear trough.

The Fort Ross Orchard contains several fruit trees planted by Russian colonists during the occupation of Fort Ross, between 1812 and 1842. The small (ca. 50 x 150 m) orchard includes olive, pear, cherry,

apple, and other fruit trees, although only a few original Russian-planted trees remain. At present, there is no information indicating the presence of original orchard trees on the northeastern side of the fault, and there does not appear to be any linear arrangements of the trees that could be used as a piercing line to measure offset across the fault. The orchard does not appear to have been maintained after abandonment by the Russian colonists, although post-1906 ranching operations included construction of a fence line across the southern part of the linear trough (B. Walton, Fort Ross State Historic Park, personal communication, 2001). Thus, the orchard likely was not being maintained during the 1906 surface rupture, and the site has undergone little cultural modification since departure of the Russians in early 1842.

### 3.0 PALEOSEISMIC RESULTS

---

During field studies in 2000 and 2004, we excavated three trenches across the fault and two fault-parallel trenches (one on each side of the fault). Our investigation in November 2000 focused on the alluvial-fan sediments in the southern part of the site (Kelson et al., 2001, 2003), and involved documentation of trench 1 across the east-facing fault scarp, trench 2 on the southwestern side of the fault, and trench 3 on the northeastern side of the fault (Figure 4). Of these, cross-fault trench 1 provides direct evidence of paleoearthquakes (as described below), whereas fault-parallel trenches 2 and 3 attempted unsuccessfully to map a possible piercing line across the fault. Results from trenches 2 and 3 are summarized in Kelson et al. (2003) and are not discussed herein. Our later work in May 2004 focused on the colluvial deposits in the northern part of the site, and involved excavation of trenches 4 and 5 across the fault bordering the linear trough (Figure 4). Correlations of deposits among trenches 1, 4, and 5 are based on deposit characteristics, relative stratigraphic position, and radiocarbon age estimates. These correlations are made between trenches that are separated by about 60 m, and are believed to be the most reasonable and stratigraphically consistent matches based on these characteristics. Collectively, the three cross-fault trenches provide evidence of four late Holocene surface ruptures at the site (Kelson et al., 2003; 2005).

#### 3.1 Stratigraphy and Structure of Trench 1

Trench 1 exposed sandstone bedrock, the San Andreas fault, and a sequence of late Holocene colluvial and alluvial sediments deposited in the linear trough northeast of the fault (Figure 5). On the southwestern side of the fault, this trench exposed sheared sandstone of the Paleocene German Rancho Formation (Wagner and Bortugno, 1982) and thin bedrock residuum (unit Cx; Figure 5). The brownish yellow to reddish yellow sandstone bedrock is pervasively sheared and weathered, and breaks out as angular to subangular fragments.

On the northeastern side of the fault, late Holocene colluvial and alluvial sediments underlie the linear trough. The oldest surficial deposit exposed in trench 1 is a silty clay with gravel (unit C2e; Figure 5) that contains reddish and orangeish sandstone clasts. These clasts are darker and more weathered than the sandstone bedrock exposed southwest of the fault, and probably were derived from the hillslope bordering the linear trough east of the fault. This lowermost deposit is overlain by beds consisting of poorly sorted silty sand with gravel (units C3e and C4e; Figure 5). These sediments also contain reddish and orangeish sandstone clasts that are as much as 4 cm in diameter, and likely were derived from the hillslope and small, southwest-trending gully northeast of the fault. The poor sorting in these deposits and absence of distinct channels suggest deposition via sheetwash, perhaps on a colluvial apron bordering the linear trough or on a small alluvial-fan surface downstream of the southwest-trending gully. These deposits are overlain by distinct, laterally discontinuous alluvial deposits of silty sand with gravel (unit A5e1; Figure 5) deposited in a northwest-trending swale. The thalweg of this channel plunges toward the closed depression northwest of trench 1, and does not cross the fault. The channel-fill deposit is conformably overlain by sandy alluvium deposited within the fault-parallel swale (unit A5e2; Figure 5).

Stratigraphically above unit A5e2 are deposits that appear to be intimately related to surface rupture along the fault (units FF6 and C7w, Figures 5 and 6). Unit FF6 consists of a triangular-shaped body within the fault zone exposed on the southeastern wall of trench 1 (station 5.5 m; Figure 5). This deposit consists of clasts of friable yellowish sandstone within a dark brown clayey sand matrix (Figure 6). The angular to subangular clasts in the deposit have near-vertical orientations, and were derived from the adjacent yellowish sandstone bedrock. Unit FF6 is interpreted as a deposit that fills a rupture-related fissure within the fault zone. This unit is distinct from overlying unit C7w based on its higher clay content, darker

color, and presence of shear fabric. Unit C7w overlies the fault zone exposed in trench 1, and is a poorly sorted colluvium derived from erosion of the northeast-facing fault scarp (Figure 5). The lithology and angularity of the gravel clasts are similar to the jointed sandstone bedrock that underlies the linear ridge. The colluvium is finer grained in an easterly direction away from the fault, and gravel clasts within the deposit are smaller and less abundant to the northeast (Figure 5). Unit C7w is not faulted, and thus represents colluvial deposition following the most-recent surface rupture at the site. Where unit C7w overlies unit FF6, it too narrows downward (Figure 6), suggesting that it also may have filled a rupture-related fissure. The absence of shearing in unit C7w contrasts with the shearing in unit FF6, and suggests that these deposits probably reflect two separate surface ruptures.

The uppermost deposits exposed in trench 1 (units A8e and C9e, Figures 5 and 6) are composed of sand with various amounts of silt, gravel, and clay. The geometry of unit A8e in the southeastern wall of trench 1 and both walls of trench 3 (Figure 4) suggests that this deposit filled a small, southeast-trending channel incised into units A5e and C4e. Unit C9e buries this deposit, and probably reflects sheetwash from the hillslope the northeast of the linear trough. Because units A8e and C9e contain barbed wire and sawn or milled pieces of redwood, they were deposited within about the past one hundred years. Directly adjacent to the present-day scarp, unit C9e grades into young scarp-derived colluvium (unit C9w) at the ground surface.

Trench 1 exposed the primary strand of the San Andreas fault, where it deforms sandstone bedrock and the surficial deposits older than unit C7w (Figure 5). In general, the N42°W-striking fault zone is only about 50 to 60 cm wide at the bottom of the trench, but it broadens to a width of about 1 m near the ground surface (Figure 5). The zone contains multiple anastomosing strands primarily within sheared bedrock, although some strands border lentic-shaped bodies of sediments (including parts of units C3e and A5e2; Figure 5). None of the fault strands exposed in trench 1 extends into unit C7w or overlying surficial deposits. Most of the fault strands extend upward to the base of unit C7w, although there are strands that extend upward only to distinct stratigraphic contacts (Figure 5). For example, on the northwestern wall of trench 1, three southwesterly dipping fault strands deform unit C2e but do not extend into unit C3e (station 6.5 m, Figure 5A). Of these three strands, the southwestern strand has a near-vertical branch that extends upward into overlying units and to the base of unit C7w. On the southeastern wall of trench 1, there are no strands that extend only to the base of unit C3e, although there is a strand that forms the contact between unit C3e and bedrock (station 6 m, Figure 5B and 6) but does not extend upward into unit C4e. Thus, upward fault terminations exist within the lower alluvium on both walls of the trench, although these terminations occur at different stratigraphic levels. On the basis of these tentative upward fault truncations and possible fissure fill (unit FF6), this trench provides possible evidence of as many as three pre-1906 ruptures (Kelson and Lettis, 2001; Kelson et al., 2003).

### **3.2 Stratigraphy and Structure of Trenches 4 and 5**

Trenches 4 and 5 were excavated about 55 and 65 m northwest of trench 1, respectively, and extended across the steep, prominent northeast-facing fault scarp (Figure 4). Our intent with this trench was to expose multiple colluvial deposits shed from the fault scarp and into the linear trough. In contrast to the southeast-trending drainage in the vicinity of trench 1, there is no integrated drainage along this part of the linear valley. Trench 4 was located near the topographically highest part of the linear trough, where the valley floor slopes very gently northwestward away from the trench (Figure 4), and is underlain primarily by colluvial material derived from both sides of the trough. Trench 5 was excavated 10 m northwest of trench 4, and extended across the steepest part of the northeast-facing fault scarp. Both trenches exposed the primary strand of the San Andreas fault where it displaces Tertiary sandstone bedrock on the southwestern side of the fault against late Holocene colluvial deposits filling the linear trough (Figure 7 and 8). As described below, these trenches provide evidence of multiple surface ruptures

based on a stacked sequence of colluvial deposits that were shed from the northeast-facing fault scarp. On the basis of deposit characteristics, stratigraphic position, radiometric age estimates, and relationships with rupture events, we correlate deposits exposed in trenches 4 and 5 with those in trench 1 (Figure 9).

Deposits exposed in trenches 4 and 5 are derived from both sides of the linear valley, primarily as a result of sheetwash colluviation from the southwest-facing hillslope bordering the trough or from degradation of the northeast-facing fault scarp. The proximity of trenches 4 and 5 and the sedimentologic similarities of deposits in the two trenches provide reasonable certainty in correlation of units between the exposures. In general, the trenches expose four packages of scarp-derived colluvial deposits, overlying older alluvium or colluvium (Figures 7 and 8), as described in more detail below. The oldest surficial deposit exposed in trenches 4 and 5 is a relatively clayey, brown colluvium within the 1-m-wide fault zone (unit Cz “Sheared colluvium”, Figures 7 and 8). This deposit is pervasively sheared and clearly has experienced multiple episodes of faulting. This clay-rich deposit is considerably firmer and denser than other deposits exposed in the trenches, and likely is substantially older. Rare charcoal samples from this deposit were not dated because its stratigraphic context is unclear.

Within the linear trough, the oldest surficial deposit is a poorly sorted sand with silt and gravel (unit C2e, Figures 7 and 8). This very dark brown deposit contains subrounded reddish and orangeish sandstone clasts as much as 4.5 cm in diameter, and common charcoal fragments in the eastern part of the trench. Poorly developed stone lines in this unit dip gently westward and indicate that this deposit was derived via sheetwash from the hillslope east of the fault. This deposit is correlated with unit C2e in trench 1 based on similar texture, color, and stratigraphic position. Directly overlying unit C2e in trenches 4 and 5 is a very dark brown, poorly sorted sand with gravel (unit C3w1; Figures 7 and 8) that contains subangular clasts of predominantly yellowish sandstone, similar to the bedrock exposed in the western part of the trench. These hard, angular to subangular clasts are as much as 7 cm in diameter, although the size and abundance of the yellowish clasts decreases eastward, away from the fault. In the central parts of trenches 4 and 5, unit C3w1 grades into unit C3e1, which contains orangeish and reddish sandstone clasts and common large charcoal fragments. Crude stone lines in unit C3e1 dip gently westward and suggest deposition via sheetwash from the hillslope east of the linear trough.

In addition, unit C3w1 grades upward into another poorly sorted silty sand with gravel (unit C3w2; Figures 7 and 8), although this overlying unit contains smaller clasts of yellowish sandstone near the fault. Just as unit C3w1 grades eastward into unit C3e1, unit C3w2 grades eastward into units C3e2 and C3e3, which contain small gravel clasts of orangeish and reddish sandstone within a sandy silt matrix. Units C3e2 and C3e3 appear to represent pulses of colluviation from the eastern hillslope. Overall, these colluvial deposits reflect upward and eastward fining of hard, angular to subangular yellowish sandstone clasts toward the center of the linear trough (a distance of only about 2 m), as well as interfingering with fairly consistent deposits containing orangeish and reddish sandstone clasts derived from the hillslope east of the fault.

A similar pattern of sediment characteristics exists for the deposits overlying units C3w2, C3e2, and C3e3. Unit C4w is adjacent to the fault and consists of poorly sorted sand with gravel (Figures 7 and 8). Clasts in this unit are hard, angular to subangular yellowish sandstone clasts as much as 8 cm in diameter, although the size and abundance of these clasts decreases eastward away from the fault. Unit C4w grades eastward into unit C4e, which contains fewer clasts but is similar to underlying unit C3e3. This pattern of sediment characteristics is repeated again in overlying unit C6w (near the fault) grading into unit C6e (away from the fault), and in unit C7w (near the fault) grading into unit C7e (away from the fault).

We interpret that all four of the colluvial deposits adjacent to the fault and on the western margin of the linear trough (i.e., units C3w, C4w, C6w, and C7w) reflect episodic uplift and scarp-production along the San Andreas fault. In trenches 4 and 5, each of these deposits is coarser and characterized by abundant angular sandstone clasts close to the fault, but is finer-grained away from the fault. In addition, each of the colluvial deposits (units C3w, C4w, C6w, and C7w, Figures 8 and 9) close to the fault has a greater concentration of clasts along its basal contact. These scarp-derived deposits grade laterally into finer grained colluvium derived from the adjacent hillslope (units C3e, C4e, C6e, and C7e, respectively). Key lithologic characteristics of these colluvial deposits are the size, color and weathering of the sandstone clasts: close to the fault the clasts are small to medium gravel of slightly weathered yellowish sandstone, whereas clasts in the northeastern parts of these colluvial deposits are very small to small pebbles of weathered reddish to orange sandstone. These characteristics, which show that the linear trough filled from both sides, allow differentiation between the scarp-derived colluvial deposits and sediments derived from the northeastern hillslope. Collectively, the sedimentologic characteristics of units C3w, C4w, C6w, and C7w suggest that repeated rejuvenation of the scarp provided a source of sandstone clasts.

The uppermost colluvial deposit (unit C7w, Figures 7 and 8) underlies the present-day ground surface about halfway up the fault scarp, and is not faulted. This unit is located downhill from a small, 15-cm-high scarplet within the overall fault scarp, which coincides with a primary fault strand that extends to the ground surface (station 2 m, Figure 8A). This scarplet continues northwestward from trench 5 for about 5 to 10 m, and probably was formed during the 1906 rupture. Unit C7w was deposited on the northeastern (downthrown) side of this scarplet, following the 1906 earthquake.

The exposures provided by trenches 4 and 5 support a depositional model that involves colluviation from both sides of the fault-parallel linear trough. The deposits indicate a relatively constant supply of colluvial material was contributed from the hillslope northeast of the trough, which interfingers with a series of scarp-derived colluvial deposits. The presence of relatively unweathered, yellowish sandstone clasts within the scarp-derived colluvial deposits (units C3w, C4w, C6w, and C7w) suggest that sandstone bedrock was exposed intermittently in the scarp face, and contributed material to the colluvial deposits. The colluvial deposits probably also were derived from the bedrock residuum present on the scarp and scarp crest (unit Cx, Figures 7 and 8). Thus, the stratigraphic characteristics of the scarp-derived colluvial deposits suggest episodic exposure of sandstone bedrock and/or clast-rich colluvial residuum. The stratigraphic relationships of units C3w, C4w, C6w, and C7w in trenches 4 and 5 indicate colluvial deposition on the northeastern side of the fault following four separate surface-rupturing earthquakes.

Both trenches 4 and 5 exposed the primary strand of the San Andreas fault, where it deforms sandstone bedrock and the surficial deposits older than unit C7w (Figures 7 and 8). As in trench 1, the primary fault zone within surficial deposits is only about 50 cm wide at the bottom of the trench, although the total zone of deformation is probably much broader and includes substantial shearing within the sandstone bedrock (Figures 7 and 8). There are multiple anastomosing fault strands within the highly deformed bedrock, as well as throughout the older colluvial deposit (unit Cz). None of the fault strands exposed in trenches 4 and 5 extends into unit C7w. Most of the major fault strands extend upward to the base of unit C7w, with the exception of several secondary strands east of the primary fault zone that die out within unit C4w. The degree of shearing along these secondary strands is substantially greater in units C3w1 than in unit C4w (Figure 8). However, trenches 4 and 5 lack evidence of upward fault truncations that may provide evidence of distinct fault ruptures.

### 3.3 Deposit Age Estimates

The age estimates for the surficial deposits at the Fort Ross Orchard site are based primarily on radiometric analyses of charcoal fragments, and secondarily on the presence of historic cultural items. Charcoal fragments were fairly abundant in several stratigraphic units, and a total of 30 charcoal samples from trenches 1 and 5 were analyzed for radiocarbon age determination (Table 1). A total of 40 analyses were conducted on these 30 charcoal fragments using conventional techniques (3 analyses) or accelerator mass spectrometry (AMS) techniques (26 analyses), supplemented by 11 AMS analyses on humic derivatives from selected duplicate samples. These analyses suggest that the composite stratigraphic record at the Fort Ross Orchard site extends from about AD 230 to the present, or about 1800 years.

Based on stratigraphic position of 14 of the 30 samples yielded age estimates that are not representative of the alluvial and colluvial deposits containing them. The presence of abundant redwood trees in the watershed, which may yield a substantial range in dates because of their long life spans and high degree of wood preservation, leads us to expect the occurrence of many non-representative age determinations in the sample population. We explicitly assume that the youngest dates are the best representation of the colluvial or alluvial deposits. The time difference between the death of each source tree and the deposition of each sample is not known. We assume that the charcoal incorporated into each colluvial or alluvial deposit was derived from the ground surface or near-surface soil/residuum directly uphill of the depositional site, such that the 2-sigma range in calibrated laboratory age adequately reflects the deposit age.

As a general rule, we interpret that the youngest radiocarbon dates from each unit best represent deposit ages. For example, we interpret that sample 1-36 (cal. AD 1630 to 1950; Table 1) best represents the age for unit A5e2, and that five separate samples reflect the age of unit C4e (Figure 10). This approach is validated by the date from sample 1-19, which was taken from a discontinuous, *in situ* burn horizon within unit C4w (Figure 5). Because the date from sample 1-19 is statistically similar to the dates from samples 1-25, 1-9, 1-15, 1-8, and 1-17 (Table 1; Figure 10), we interpret that the youngest dates from any given unit generally best reflect the age of that deposit. Based on this approach, 16 of the 30 samples yielded representative ages (Figure 10), and these dates were used in the OxCal analytical program (Ramsey, 1995, 2001, 2005).

In contrast, sample 5-3 from unit C4w and sample 1-42 from unit C2e appear to be anomalously young for their respective deposits, relative to dates from other adjacent deposits. Although we observed no evidence of animal burrowing or modern tree roots in the vicinity of sample 5-3 (Figure 8), this sample yielded essentially a modern date, which is strongly inconsistent with several older clustered dates from overlying deposits (including sample 1-19 from the *in situ* burn). We interpret that this charcoal fragment is not representative of deposit age because it is anomalously young. Similarly, we interpret that the date from sample 1-42 is anomalously young for unit C2e. This sample probably was intruded into unit C2e during or after deposition of unit C3e, and probably is not representative of the age of unit C2e. Because the 16 highlighted age estimates shown on Figure 10 are reasonably consistent with stratigraphic position, we used these dates in our analysis of deposit age and rupture chronology using the OxCal program (Ramsey, 2005), as described below.

Table 1. Summary of Radiocarbon Analyses, Fort Ross Orchard Site

Sample No.	Lab No. <sup>®</sup>	Duplicate 1	Duplicate 2	Duplicate 3	Weighted Avg	Calibrated Age (yr AD, >95%) <sup>#</sup>	Sample No.	Lab No. <sup>®</sup>	<sup>14</sup> C Age (yr BP ± 1s)	Calibrated Age (yr AD, >95%) <sup>#</sup>
		<sup>14</sup> C Age (yr BP ± 1s)	<sup>14</sup> C Age* (yr BP ± 1s)	<sup>14</sup> C Age* (yr BP ± 1s)	Radiocarbon Age * (yr BP ± 1s)					
<b>Trench 1 (Year 2000)</b>						<b>Trench 5 (Year 2004)</b>				
<b>Unit C7w: Scarp-derived Colluvium</b>						<b>Unit C7w: Scarp-derived Colluvium</b>				
FRT1-12	CAMS 71277, 77386	200 ± 40			190 ± 35	AD 1650 to 1950	no samples analyzed			
FRT1-57	CAMS 76671, 76732	(740 ± 50)	(670 ± 60)		(710 ± 40)	(AD 1260 to 1390)				
1906 EQ										
<b>Unit FF6 :Fissure Fill</b>						<b>Unit C6w: Scarp-derived Colluvium</b>				
FRT1-54	CAMS 76672, 76733	(3420 ± 150)	(700 ± 30)		(700 ± 30)	(AD 1270 to 1380)	FRT5-14	AA60714	127±30	AD 1670 to 1960
							FRT5-13	AA60713	187±30	AD 1650 to 1950
							FRT5-35	AA60719	(512±38)	(AD 1330 to 1440)
Event 2										
<b>Unit A5e2: Alluvium</b>										
FRT1-36	CAMS 76673	210 ± 40			210 ± 40	AD 1630 to 1950				
FRT1-13	CAMS 71524	(800 ± 40)			(800 ± 40)	(AD 1180 to 1280)				
FRT1-23	CAMS 77378	(530 ± 50)			(530 ± 50)	(AD 1300 to 1450)				
<b>Unit A5e1: Alluvium</b>										
FRT1-25	CAMS 77379, 77389	390 ± 50	370 ± 50		380 ± 35	AD 1440 to 1540				
<b>Unit C4e: Hillslope Colluvium</b>										
FRT1-9	CAMS 71274, 77387	330 ± 40	310 ± 50		320 ± 30	AD 1480 to 1650				
FRT1-15	CAMS 71525	310 ± 40			310 ± 40	AD 1470 to 1660				
FRT1-8	CAMS 71273, 71280, 71281	360 ± 50	390 ± 40	430 ± 50	390 ± 30	AD 1440 to 1630				
FRT1-11	CAMS 71276, 77385	(650 ± 40)	(620 ± 50)		(640 ± 35)	(AD 1290 to 1400)	<b>Unit C4w: Scarp-derived Colluvium</b>			
FRT1-19	CAMS 71528	320 ± 40			320 ± 40	AD 1460 to 1660	FRT5-24	AA60717	725±40	AD 1220 to 1380
FRT1-17	CAMS 71527	370 ± 40			370 ± 40	AD 1440 to 1640	FRT5-15	AA60715	(1509±39)	(AD 430 to 640)
FRT1-46	CAMS 76674	(910 ± 60)			(910 ± 60)	(AD 1020 to 1250)	FRT5-3	Beta193488	(50±40)	(AD 1690 to 1950)
							FRT5-9	AA60712	(1245±40)	(AD 670 to 890)
Event 3										
<b>Unit C3e: Hillslope Colluvium</b>						<b>Unit C3w: Scarp-derived Colluvium</b>				
FRT1-45	CAMS 76734, 76948		(1030 ± 40)	(1060 ± 50)	(1040 ± 35)	(AD 900 to 1030)	FRT5-19	AA60716	(1751±49)	(AD 130 to 410)
FRT1-10	CAMS 71275, 77384	(1130 ± 40)	(1270 ± 60)		(1175 ± 35)	(AD 780 to 980)	FRT5-2	Beta193487	950±60	AD 980 to 1200
FRT1-16	CAMS 71526	770 ± 40			770 ± 40	AD 1190 to 1290	FRT5-29	AA60718	889±38	(AD 1030 to 1240)
							FRT5-7	Beta193489	990±50	AD 900 to 1190
Event 4										
<b>Unit C2e: Hillslope Colluvium</b>						<b>Unit C2e: Hillslope Colluvium</b>				
FRT1-42	CAMS 76675	(720 ± 40)			(720 ± 40)	(AD 1190 to 1280)	no samples analyzed			
FRT1-20	CAMS 71614	1730 ± 40			1730 ± 40	AD 230 to 420				

Samples are listed in stratigraphic order, with stratigraphically highest samples at the top.

@ Lab ID: CAMS = Center for Accelerator Mass Spectrometry, Lawrence Livermore National Laboratory (AMS technique)

AA = University of Arizona (AMS technique)

Beta = Beta Analytic, Inc., Miami, Florida (Conventional technique)

\* Duplicate samples from Trench 1 analyzed on humic derivatives (G. Seitz, LLNL, personal comm., 2001). In all cases except FRT1-54, duplicate ages are statistically correlative (R=0.98) with AA

^ Samples weighted equally

# Calibrated based on Stuiver and Reimer (1993) using CALIB v4.3 (2000); or based on Stuiver et al. (1998) by Beta Analytic.

() Parentheses indicate stratigraphically inconsistent age determinations.

#### 4.0 NUMBER AND TIMING OF SURFACE-RUPTURING EARTHQUAKES

---

The stratigraphic relationships exposed in trenches 1, 4, and 5 provide evidence of multiple late Holocene surface-rupturing earthquakes at this site. The characteristics of units C3w, C4w, C6w, and C7w in trenches 4 and 5 strongly suggest colluvial deposition following four separate surface-rupturing earthquakes at the site. Assuming that the radiocarbon ages reflect the age of the colluvial deposits (as discussed above), the estimated ages of these deposits probably closely reflect the timing of individual ruptures. Trench 1 provides supporting evidence of these late Holocene surface ruptures (Kelson et al., 2003). Thus, we interpret the occurrence of four large, surface-rupturing earthquakes within the past approximately 1800 years at the Fort Ross Orchard site, including the 1906 earthquake, the penultimate earthquake (Event 2), and earlier earthquakes (Events 3 and 4) (Table 2).

We use the OxCal calibration and analysis program (Ramsey, 2005) to help interpret the ages of surficial deposits and the timing of earthquake ruptures at the Fort Ross Orchard site. This program uses stratigraphic relations among deposits and Bayesian statistics applied to deposit ages to develop probability density functions for ages of inter-deposit “events”. In our analysis, these “events” are surface ruptures that resulted in specific deposits at the site. As noted above, we selected 16 radiocarbon dates that are assumed to best represent the ages of deposits (Figure 10). The laboratory ages of these deposits were calibrated to the tree-ring record by the OxCal program (v 3.9; Ramsey, 2003), and then used to construct an appropriate analytical model that consists of eight separate depositional phases encompassing four surface-rupture “events” (Figure 11). The dates between and within each phase were sequenced in the model based on stratigraphic position (Table 1), and analysis of dates from the phases bracketing each event provides estimates of the timing of the surface ruptures. Our OxCal analytical model first used only dates from trench 1, then only dates from trench 5, and finally dates from both trenches in a combined model (Table 2). The combined data from trenches 1 and 5 provide better constraint on the event timing, and is summarized below.

On the basis of the calibrated radiocarbon dates, Event 4 occurred after deposition of unit C2e but before colluvial deposit C3w and, based on the combined record from trenches 1 and 5 (Table 2), occurred between AD 300 and 1050 (Figure 11). Using the same analytical model, the available radiocarbon dates yield an age range for Event 3 of between AD 1210 and 1380, and the penultimate rupture (Event 2) occurred between AD 1630 and 1820 (Table 2). The estimated timing of the penultimate earthquake prior to AD 1820 is consistent with historical records. There are no known references by Russian colonists at Fort Ross to a large earthquake during their tenure in the area between AD 1812 and 1842. In addition, there was an absence of large earthquakes in the San Francisco Bay region between 1776 and 1838, as suggested by records from Mission Dolores in downtown San Francisco (Toppozada and Borchardt, 1998). Therefore, this historical information is used to limit the latest date of the penultimate surface-rupture earthquake at Fort Ross Orchard (Table 2).

We interpret that the sheared fissure fill deposit (unit FF6; Figure 6) was formed following the penultimate event, although we cannot preclude that it formed following Event 3. We favor the interpretation that unit FF6 formed from Event 2 because it is overlain directly by the unfaulted colluvial deposit (unit C7w), which was formed soon after the 1906 earthquake. Unit C7w appears to have filled a smaller, less distinct depression along the fault directly above unit FF6 (Figure 6). If unit FF6 had been formed by Event 3, we infer that Event 2 would probably also have produced a fissure or small depression at the same location. The absence of an intermediate fissure-fill deposit between units FF6 and C7w suggest that unit FF6 was formed during the penultimate rupture.

Table 2. Age estimates for four most-recent surface-rupturing earthquakes on the North Coast section of the San Andreas fault at the Fort Ross Orchard site. Age ranges represent uncertainty levels estimated by the OxCal analytical program (Ramsey, 2003).

<b>Earthquake Rupture</b>	<b>Trench 1 only (2-sigma range)</b>	<b>Trench 5 only (2-sigma range)</b>	<b>Trenches 1 and 5 combined (2-sigma range)*</b>
1906	AD 1906	AD 1906	<b>AD 1906</b>
Event 2	AD 1680 to 1910	AD 1280 to 1750	<b>AD 1630 to 1776</b>
Event 3	AD 1230 to 1490	AD 1090 to 1340	<b>AD 1210 to 1380</b>
Event 4	AD 300 to 1250	Prior to AD 1060	<b>AD 300 to 1050</b>

\* Timing of Event 2 truncated at AD 1776 based on historical records (Topozada and Borchardt, 1998).

Lastly, we interpret that deposition of scarp-derived colluvial unit C7w closely followed the 1906 rupture, because it overlies the fault zone and is not faulted. In addition, deposition of units A8e and C9e contain historical cultural items (e.g., nails, sawn wood pieces), and thus are less than one hundred years old. The production of a northeast-facing fault scarp during 1906 is supported the observations of F. Matthes (summarized in Lawson, 1908) (Figure 2).

## 5.0 COMPARISON WITH PUBLISHED NORTH COAST RUPTURE CHRONOLOGIES

---

The WGCEP (2003) interprets that the northern San Andreas fault (north of San Juan Bautista) consists of four segments: the Offshore segment from Cape Mendocino south to Point Arena, the North Coast segment from Point Arena to the Golden Gate, the Peninsula segment from the Golden Gate to Los Gatos, and the Santa Cruz Mountains segment from Los Gatos to San Juan Bautista (Figure 1). The history of past earthquakes on these segments is based on paleoseismologic studies at a dozen or so onshore sites, and a series of offshore core sites (Figure 12). Recent and ongoing development of additional paleoseismologic data allows for refinement of previous rupture chronologies (Hall et al., 1999; Schwartz et al., 1998; Knudsen et al., 2002), and leads to a better understanding of rupture segmentation and the long-term behavior of the fault. Many recent studies collectively provide an emerging picture of how the fault ruptures in time and space. Figure 12 provides a summary of event chronologies available at the time of this writing, organized by distance along the fault from Cape Mendocino to San Juan Bautista. As discussed below, information developed at the Fort Ross Orchard site helps refine the collective chronology along the North Coast segment, and suggests that the three or four most-recent surface ruptures at Fort Ross occurred on the North Coast segment but not necessarily on adjacent fault segments.

The Fort Ross Archae Camp site (Figure 2) provides broadly constrained information on the timing of the past four surface ruptures on the North Coast segment (Noller et al., 1993; Simpson et al., 1996; Noller and Lightfoot, 1997). Two trenches excavated in 1992 showed the presence of three pre-1906 deposits interpreted to be scarp-derived colluviums, and provided limited radiometric, obsidian-hydration, and archaeological data to address event timing (Noller et al., 1993). Two trenches excavated in 1994 showed a series of slope deposits that also were interpreted to be related to surface-rupture events (Simpson et al., 1996). The age estimates of surface ruptures interpreted by Simpson et al. (1996) are given in Table 3. Based on our field experience at the Archae Camp site, we re-analyzed the limited age estimates available for the Archae Camp site using the OxCal program to compare the event chronology with the Fort Ross Orchard site. As shown on Table 3, the timing of the penultimate event at Archae Camp (“Event Y” of Simpson et al., 1996) does not coincide with Event 2 at Fort Ross Orchard. We interpret that that Event 2 was not recorded or possibly not recognized at the Archae Camp site, and allow the OxCal model to assign a very broad range (AD 1570 to 1906) for this event. Events “X” and “W” identified at Archae Camp overlap in time with Events 3 and 4, respectively, at Fort Ross Orchard (Table 3). The Archae Camp site therefore confirms the rupture chronology identified in trenches at Fort Ross Orchard, and substantially decreases the uncertainty in the age-range for Event 4 (Table 3). Based on the combined record from Fort Ross Orchard and Archae Camp, we interpret the occurrence of four late Holocene surface ruptures on the North Coast segment of the San Andreas fault within the past approximately 1100 years (Figure 12).

This event chronology coincides favorably with data from other sites along the North Coast segment (Figure 12). For example, the Scaramella Ranch site near Point Arena provides evidence of a rupture after AD 1530 (Prentice, 1989), which is consistent with a similar, broad range from Bodega Harbor (Knudsen et al., 2002). The stratigraphic record at the Bolinas Lagoon site does not indicate an event during this time interval, although the marsh stratigraphy does not preclude the occurrence of a rupture during the time frame (R. Witter, personal comm., 2005). Collectively, these data support the occurrence of a surface rupture in the 17<sup>th</sup> or 18<sup>th</sup> century that extended at least from Point Arena to Olema, and probably ruptured the entire North Coast segment. No evidence of rupture during this time frame at the Filoli and Grizzly Flat sites (Hall et al., 1999; Schwartz et al., 1998) raises the possibility that this rupture did not extend south of the Golden Gate (Figure 12).

Table 3. Summary of age estimates for recent surface-rupturing earthquakes on the San Andreas fault at the Archae Camp and Fort Ross Orchard sites. Age ranges represent uncertainty levels estimated by the OxCal analytical program (Ramsey, 2003).

<b>Archae Camp (Simpson et al., 1996)</b>	<b>Archae Camp OxCal revision (2-sigma range)</b>	<b>Fort Ross Orchard (2-sigma range)*</b>	<b>Fort Ross Orchard and Archae Camp (2-sigma range)*</b>
(Event Z) AD 1906	AD 1906	AD 1906	<b>AD 1906</b>
	(Event 2) AD 1570 to 1906	(Event 2) AD 1630 to 1776	<b>(Event 2) AD 1630 to 1776</b>
(Event Y) AD 1170 to 1650	(Event 3) AD 1220 to 1560	(Event 3) AD 1210 to 1380	<b>(Event 3) AD 1210 to 1380</b>
(Event X) AD 920 to 1285	(Event 4) AD 920 to 1230	(Event 4) AD 300 to 1050	<b>(Event 4) AD 920 to 1050</b>
(Event W) AD 555 to 950	(Event 5) AD 600 to 880		

\* Timing of Event 2 truncated at AD 1776 based on historical records (Topozada and Borchardt, 1998).

Stratigraphic evidence of Event 3 at Fort Ross Orchard suggests a rupture between about AD 1210 and 1380 (Table 2). This range is consistent with broad ranges from the Archae Camp site (Figure 12), and from the Alder Creek and Scaramella Ranch sites near Point Arena (Baldwin, 1996; Baldwin et al., 2000; Prentice 1989; Prentice et al., 1999). Considering the broad age range for Event 3 estimated from Bodega Harbor and Bolinas Lagoon (Knudsen et al., 2002), the Fort Ross data provide the current best estimate for the Event 3 rupture along the North Coast segment.

Recent research on the offshore turbidite record provides preliminary data on possible ruptures along the San Andreas Offshore and North Coast segments (Goldfinger et al., 2003a, b), which documents the occurrence of five episodes of turbidite deposition within the past thousand years or so at the Noyo Canyon core site (Figure 1). These events are interpreted to be the result of five paleoearthquakes (Figure 12), some of which may have occurred along the North Coast or Offshore segments of the San Andreas fault. Great earthquakes along the Cascadia subduction zone also may have contributed to the turbidite record interpreted from the Noyo Canyon core. Goldfinger et al. (2003a) use these initial data to interpret that a large earthquake occurred between AD 1505 and 1820 (Figure 12), presumably on the northern San Andreas fault. This range is consistent with our age-range of AD 1630 to 1820 from Fort Ross and similar ages from other onshore North Coast sites. Goldfinger et al. (2003a) interpret two additional events between 1445 and 1665 AD, which do not coincide with Event 3 based on the collective North Coast record (Figure 12). We speculate that if these two turbidite events are related to strong ground motions from a large earthquake, they may represent events on either the nearby San Andreas Offshore segment or the more-distant Cascadia subduction zone, rather than the North Coast segment. The preliminary turbidite record also yields events that may coincide with Event 3 and 4 identified from the onshore record along the North Coast segment (Figure 12). In summary, the latest Holocene surface-rupture chronology interpreted from the Fort Ross Orchard site is consistent with data from multiple paleoseismic sites elsewhere along the North Coast segment, but not necessarily consistent with the preliminary record from turbidite studies.

The occurrence of the 1906 earthquake along the entire northern San Andreas fault (Lawson, 1908), and the 1838 earthquake along only the Peninsula fault segment (Toppozada and Borchardt, 1998), demonstrates that the northern San Andreas fault may rupture along all or just some of its 470 km length. The rupture chronology provided by the studies at Fort Ross and other sites along the North Coast segment suggest that ruptures may occur along the full length of this segment. However, paleoseismic data are insufficient to demonstrate that smaller ruptures could occur within this segment. In addition, available paleoseismic data from onshore and offshore studies on other fault segments also are insufficient at this time to address the temporal pattern of ruptures along the entire northern San Andreas fault. Although the behavior of the northern San Andreas fault probably involves a mix of large, long ruptures like the 1906 event and smaller ruptures along shorter segments of the fault, additional information on the late Holocene history of rupture events at several sites along the northern San Andreas fault is needed to better understand the behavior of this major plate boundary.

## 6.0 CONCLUSIONS

---

Paleoseismic trenching within Fort Ross State Historic Park provides data on the late Holocene rupture history of the North Coast segment of the northern San Andreas fault. Trenches across the northeast-facing fault scarp at the Fort Ross Orchard site provide stratigraphic and structural evidence of the 1906 earthquake and three pre-1906 surface ruptures. These trenches show the presence of scarp-derived colluvial deposits, possible fissure-fill deposits, and tentative upward fault truncations that provide evidence of three possible surface ruptures prior to 1906. Coarse-grained scarp-derived colluvial sediments shed from the scarp after individual surface-rupturing earthquakes pre-date the 1906 rupture and constrain the timing of earthquakes over the past approximately 1100 years. Correlation of deposits among the trenches is based on lithologic characteristics, stratigraphic position, and a total of 40 radiometric analyses of charcoal fragments. Based on stratigraphic ordering and a statistical comparison of radiocarbon dates using the OxCal program, the past four surface ruptures at the Fort Ross Orchard site occurred within these ranges: AD 1906, AD 1630 to 1776, AD 1210 to 1380, and AD 300 to 1050. Our re-analysis of radiocarbon ages from the nearby Archae Camp site (Simpson et al., 1996) are consistent with these dates, and further constrain the earliest of this series to have occurred between AD 920 and 1050.

The time windows for late Holocene ruptures at Fort Ross are consistent with results from several other sites on the North Coast segment of the fault, although published paleoseismic data are, at present, insufficient to address the long-term behavior of the entire northern San Andreas fault. The behavior of the northern San Andreas fault probably involves a mix of large, long ruptures like the 1906 event and smaller ruptures along shorter segments of the fault. However, additional information on the late Holocene history of rupture events at several sites along the northern San Andreas fault is needed to better understand the behavior of this major plate boundary.

## 7.0 ACKNOWLEDGEMENTS

---

This research was supported by the U.S. Geological Survey (USGS), Department of the Interior, under USGS award numbers 01-HQ-GR-0072 and 02-HQ-GR-0069. The views and conclusions contained in this document are those of the authors and should not be interpreted as necessarily representing the official policies, either expressed or implied, of the U.S. Government. The California Department of Parks and Recreation graciously provided permission to conduct this investigation within the Fort Ross State Historic Park, following archaeological and environmental clearance. Thanks especially to California Department of Parks and Recreation personnel Bill Walton, Heidi Horvitz, Breck Parkman, and Dan Murley. Cres Creswell of the village of Seaview ably excavated and backfilled all the trenches, and Graham Daldorff of the Anthropological Studies Center (Sonoma State University) provided archaeological monitoring of the excavations. Thanks also to Carol Prentice, David Schwartz, Tom Fumal, Chris Crosby, Heidi Stenner, Tim Dawson, and Judy Zachariason (U.S. Geological Survey), John Baldwin, Rob Witter and William Lettis (WLA), Koji Okimura (Hiroshima University), Rich Briggs (Center for Neotectonics Studies, Reno), and Omer Emre (Turkish Mineral Research and Exploration) for providing insightful field and office discussions. Our appreciation also goes to Gordon Seitz and John Southon (Center for Accelerator Mass Spectrometry, Lawrence Livermore National Laboratories), Darden Hood (Beta Analytic, Inc.), and George Burr (NSF-Arizona AMS Laboratory at the University of Arizona) for completing radiometric analyses.

## 8.0 REFERENCES

---

- Baldwin, J.N., 1996, Paleoseismic investigation of the San Andreas fault on the north coast segment, near Manchester, California: M.S. thesis, San Jose State University, San Jose, California, 127 p.
- Baldwin, J.N., Knudsen, K.L., Lee, A., Prentice, C.S., and Gross, R., 2000, Preliminary estimate of coseismic displacement of the penultimate earthquake on the northern San Andreas fault, Pt. Arena, California: *in* Bokelman, G., and Kovachs, R. (eds.), Tectonic problems of the San Andreas fault system, Stanford University Publications, p. 355-368.
- Brown, R.D., and Wolfe, E.W., 1970, Map showing recently active breaks along the San Andreas fault between Point Delgada and Bolinas Bay, California: U.S. Geological Survey Miscellaneous Field Investigations Map I-692, scale 1:24,000.
- Fumal, T.E., Heingartner, G.F., and Schwartz, D.P., 1999, Timing and slip of large earthquakes on the San Andreas fault, Santa Cruz Mountains, California [abs.]: Geological Society of America Abstracts with Programs, v. 31, no. 6, p. A-56.
- Goldfinger, C., Nelson, C.H., Johnson, J.E., and The Shipboard Scientific Party, 2003a, Holocene earthquake records from the Cascadia subduction zone and northern San Andreas fault based on precise dating of offshore turbidites: Annual Reviews of Earth and Planetary Science, v. 31, pp. 555-577.
- Goldfinger, C., Nelson, C.H., Johnson, J.E., and The Shipboard Scientific Party, 2003b, Deep-water turbidites as Holocene earthquake proxies: the Cascadia subduction zone and northern San Andreas fault systems: Annals of Geophysics, v. 46, no. 5, pp. 1169-1194.
- Hall, N.T., Wright, R. H., and Clahan, K. B., 1999, Paleoseismic studies of the San Francisco Peninsula segment of the San Andreas fault zone near Woodside, California: Journal of Geophysical Research, v. 104, no. B10, p. 23,215-23,236.
- Kelson, K.I., and Lettis, W.R., 2001, Evaluation of paleoearthquakes along the northern San Andreas fault, Fort Ross State Historic Park, California: Annual Project Summary submitted to the U.S. Geological Survey National Earthquake Hazard Reduction Program <[http://erp-web.er.usgs.gov/reports/annsum/vol42/nc/nc\\_vol42.htm](http://erp-web.er.usgs.gov/reports/annsum/vol42/nc/nc_vol42.htm)>.
- Kelson, K.I., Koehler, R.D., and Kang, K.-H., 2003, Initial evaluation of paleoearthquake timing on the northern San Andreas fault at the Fort Ross Orchard site, Sonoma County, California: Final Technical Report submitted to the U.S. Geological Survey National Earthquake Hazard Reduction Program, Award No. 00HQGR0072, 29 p.
- Kelson, K.I., Streig, A., and Koehler, R.D., 2005, Preliminary Evaluation of Paleoseismicity Timing, northern San Andreas Fault, Fort Ross, CA [abs.]: Geological Society of America Abstracts with Programs, vol. 37, no. 4; San Jose, California, to be presented May 1, 2005.
- Knudsen, K.L., Witter, R.C., Garrison-Laney, C.E., Baldwin, J.N., and Carver, G.A., 2002, Past earthquake-induced rapid subsidence along the northern San Andreas fault: A paleoseismological method for investigating strike-slip faults: Bulletin of the Seismological Society of America, v. 92, no. 7, p. 2612-2636.
- Lawson, A.C., 1908, The California earthquake of April 18, 1906: Report of the State Earthquake Investigation Commission (Reprinted 1969), v. 1, Carnegie Institution of Washington Publication, 451 p. and atlas.

- Muhs, D.R., Prentice, C., and Merritts, D.J., 2003, Marine terraces, sea level history, and Quaternary tectonics of the San Andreas fault on the coast of California: *in* Easterbrook, D., ed., Quaternary Geology of the United States, INQUA 2003 Field Guide Volume, Desert Research Institute, Reno, NV, p. 1-18.
- Niemi, T.M., and Hall, N.T., 1992, Late Holocene slip rate and recurrence of great earthquakes on the San Andreas fault in northern California: *Geology*, v. 20, p. 195-198.
- Niemi, T.M., Zhang, H., Generaux, S., Fumal, T. and Seitz, G., 2002, A 2500-year record of earthquakes along the northern San Andreas fault at Vedanta Marsh, Olema, CA [abs]: Geological Society of America Cordilleran Section, 98<sup>th</sup> Annual Meeting Abstracts With Programs, v. 34, no. 5, p. 86.
- Niemi, T.M., Zhang, H., and Generaux, S., 2003, Determination of a high resolution paleoearthquake chronology for the northern San Andreas fault at the Vedanta Marsh site, Marin County, CA: Annual Project Summary submitted to the U.S. Geologic Survey National Earthquake Hazards Reduction Program, Award No. 03HQGR0015, 7 p.; <http://erp-web.er.usgs.gov/reports/annsum/vol45/nc/03HQGR0015annb.pdf>.
- Niemi, T.M., Zhang, H., and Fumal, T.E., 2005 (in preparation), Determination of a high resolution paleoearthquake chronology for the northern San Andreas fault at the Vedanta Marsh site, Marin County, CA: USGS/NEHRP Final Technical Report, Grant No. 03HQGR0015.
- Noller, J.S., Kelson, K.I., Lettis, W.R., Wickens, K.A., Simpson, G.D., Lightfoot, K., Wake, T., 1993, Preliminary characterizations of Holocene activity on the San Andreas fault based on offset archaeological sites, Ft. Ross State Historic Park, California: Final Technical Report submitted to the U.S. Geologic Survey National Earthquake Hazards Reduction Program, 17 p.
- Noller, J.S., and Lightfoot, K.G., 1997, An archaeoseismic approach and method for the study of active strike-slip faults: *Geoarchaeology: An International Journal*, v. 12, p. 117-135.
- Prentice, C.S., 1989, Earthquake geology of the northern San Andreas fault near Point Arena, California: Pasadena, California, California Institute of Technology, Ph.D. Dissertation, 252 p.
- Prentice, C.S., Langridge, R., and Merritts, D.J., 2000, Paleoseismic and Quaternary tectonic studies of the San Andreas fault from Shelter Cove to Fort Ross: *in* Bokelman, G., and Kovachs, R. (eds.), Tectonic problems of the San Andreas fault system, Stanford University Publications, p. 349-351.
- Prentice, C.S., Merritts, D.J., Beutner, E.C., Bodin, P., Schill, A., and Muller, J.R., 1999, Northern San Andreas fault near Shelter Cove, California: *Geological Society of America Bulletin*, v. 111, no. 4, p. 512-523.
- Prentice, C.S., Prescott, W.H., and Langridge, R., 2001, New geologic and geodetic slip rate estimates on the North Coast San Andreas fault: Approaching agreement? [abs]: *Seismological Research Letters*, v. 72, no. 2, p. 282.
- Ramsey, C.B., 1995, Radiocarbon Calibration and Analysis of Stratigraphy: The OxCal Program: *Radiocarbon*, v. 37, no. 2, p. 425-430.
- Ramsey, C.B., 2001, Development of the Radiocarbon Program OxCal, *Radiocarbon*, v. 43, no. 2A, p. 355-363.
- Ramsey, C.B., 2005, Radiocarbon Calibration and Analysis of Stratigraphy: The OxCal Program v3.10: <<http://www.rlaha.ox.ac.uk/oxcal>>

- Schwartz, D.P., Pantosti, D., Okumura, K., Powers, T.J., and Hamilton, J.C., 1998, Paleoseismic investigations in the Santa Cruz Mountains, California: Implications for recurrence of large-magnitude earthquakes on the San Andreas fault: *Journal of Geophysical Research*, v. 103, p. 17,985-18,001.
- Simpson, G.D., Noller, J.S., Kelson, K.I., and Lettis, W.R., 1996, Logs of trenches across the San Andreas fault, Archae Camp, Fort Ross State Historic Park, Northern California: Final Technical Report submitted to the U.S. Geologic Survey National Earthquake Hazards Reduction Program, Award No. 1434-94-G-2474, 1 plate.
- Stuiver, M., and Reimer, P.J., 1993, Extended  $^{14}\text{C}$  data base and revised CALIB 3.0  $^{14}\text{C}$  age calibration program: *Radiocarbon*, v. 35, p. 215-230.
- Stuiver, M., Reimer, P.J., and Braziunas, T. F. 1998, High-precision radiocarbon age calibration for terrestrial and marine samples: *Radiocarbon*, v. 40, p.1127-1151.
- Thatcher, W., Marshall, G., and Lisowski, M., 1997, Resolution of fault slip along the 470-km-long rupture of the great 1906 San Francisco earthquake and its implications: *Journal of Geophysical Research*, v. 102, no. B3, p. 5353-5367.
- Topozada, T.R., and Borchardt, G., 1998, Re-evaluation of the 1836 "Hayward Fault" and the 1838 San Andreas fault earthquakes: *Bulleting of the Seismological Society of America*, v. 88, p. 140-159.
- Wagner, D.L., and Bortugno, E.J., 1982, Geologic Map of the Santa Rosa Quadrangle, California: California Division of Mines and Geology, Regional Geologic Map Series, Santa Rosa Quadrangle, Map 2A (Geology), Sheet 1 of 5, scale 1:250,000.
- Working Group on California Earthquake Probabilities (WGCEP), 1999, Probabilities of large earthquakes in the San Francisco Bay region, California: U.S. Geological Survey Open-file Report 99-517.
- Working Group on California Earthquake Probabilities (WGCEP), 2003, Earthquake probabilities in the San Francisco Bay region: 2002 to 2031--A summary of findings: U.S. Geological Survey Open-file Report 03-214.
- Zhang, H., Niemi, T.M., Allison, A., and Fumal, T., 2004, Noncharacteristic slip on the northern San Andreas fault at the Vedanta Marsh, Marin County, CA: *Eos. Trans. AGU*, 85 (47), Fall Meeting Supplement, Abstract T13C-1395.

## Figures

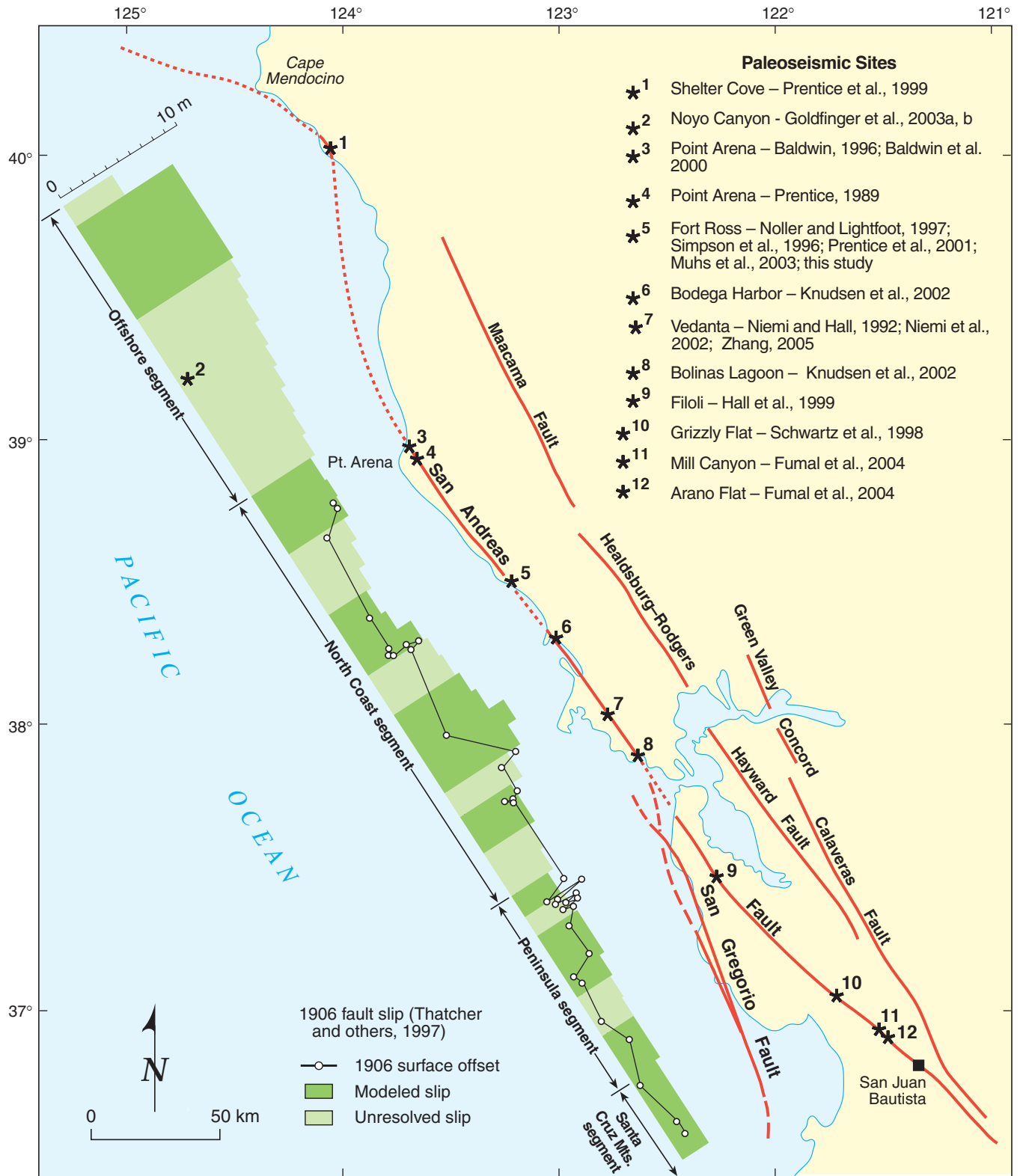


Figure 1. Regional map of major faults in northwestern California, showing San Andreas fault segments from WGCEP (2003), previous paleoseismic sites, and the distribution of surface and geodetic slip produced by the 1906 rupture (Thatcher et al., 1997).

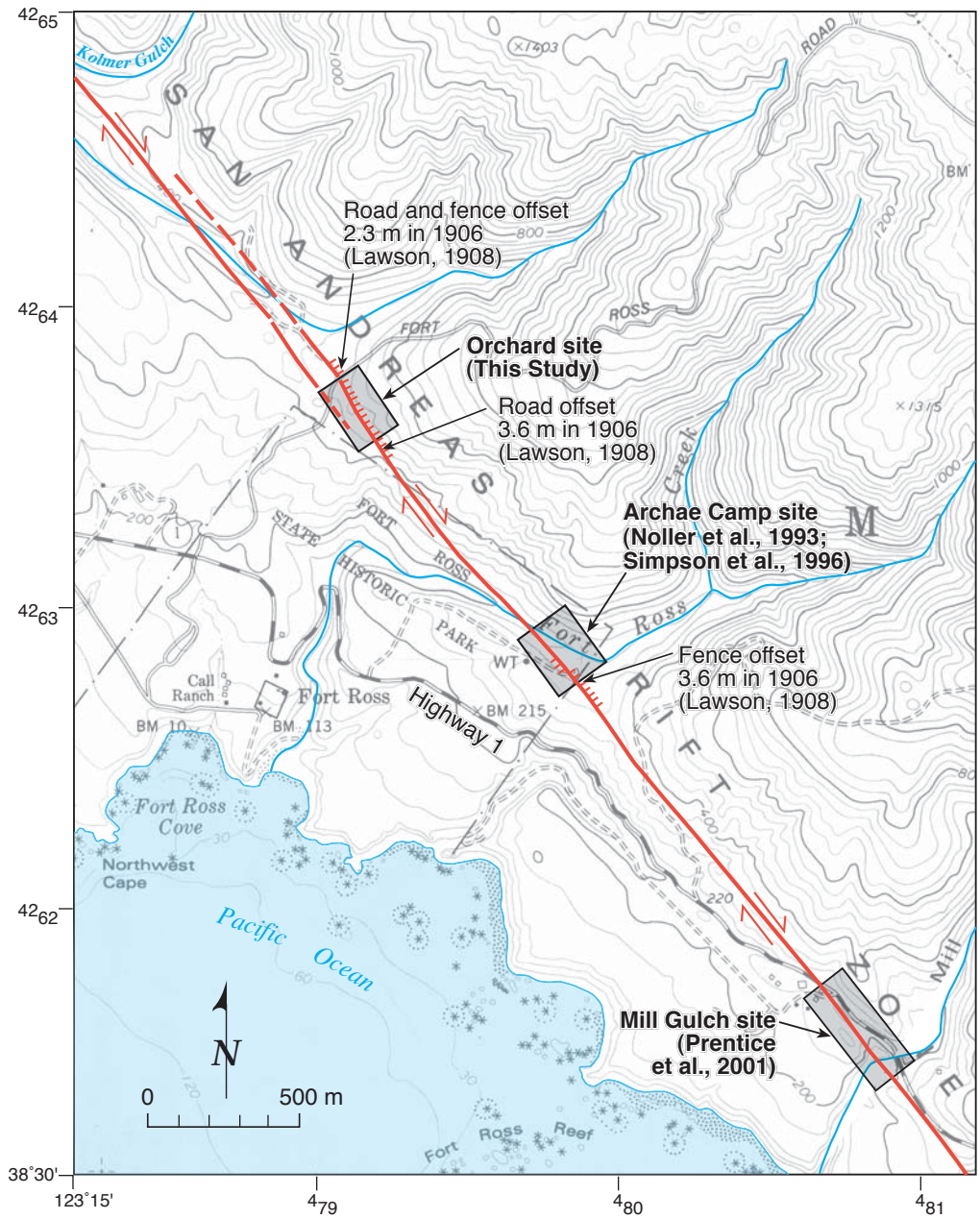


Figure 2. Topographic map of the Fort Ross area, showing locations of recent paleoseismic sites on the San Andreas fault and documented offsets from the 1906 earthquake.



Figure 3. Photograph of trenches 4 and 5 at the Fort Ross Orchard site, looking southwest across the San Andreas fault.

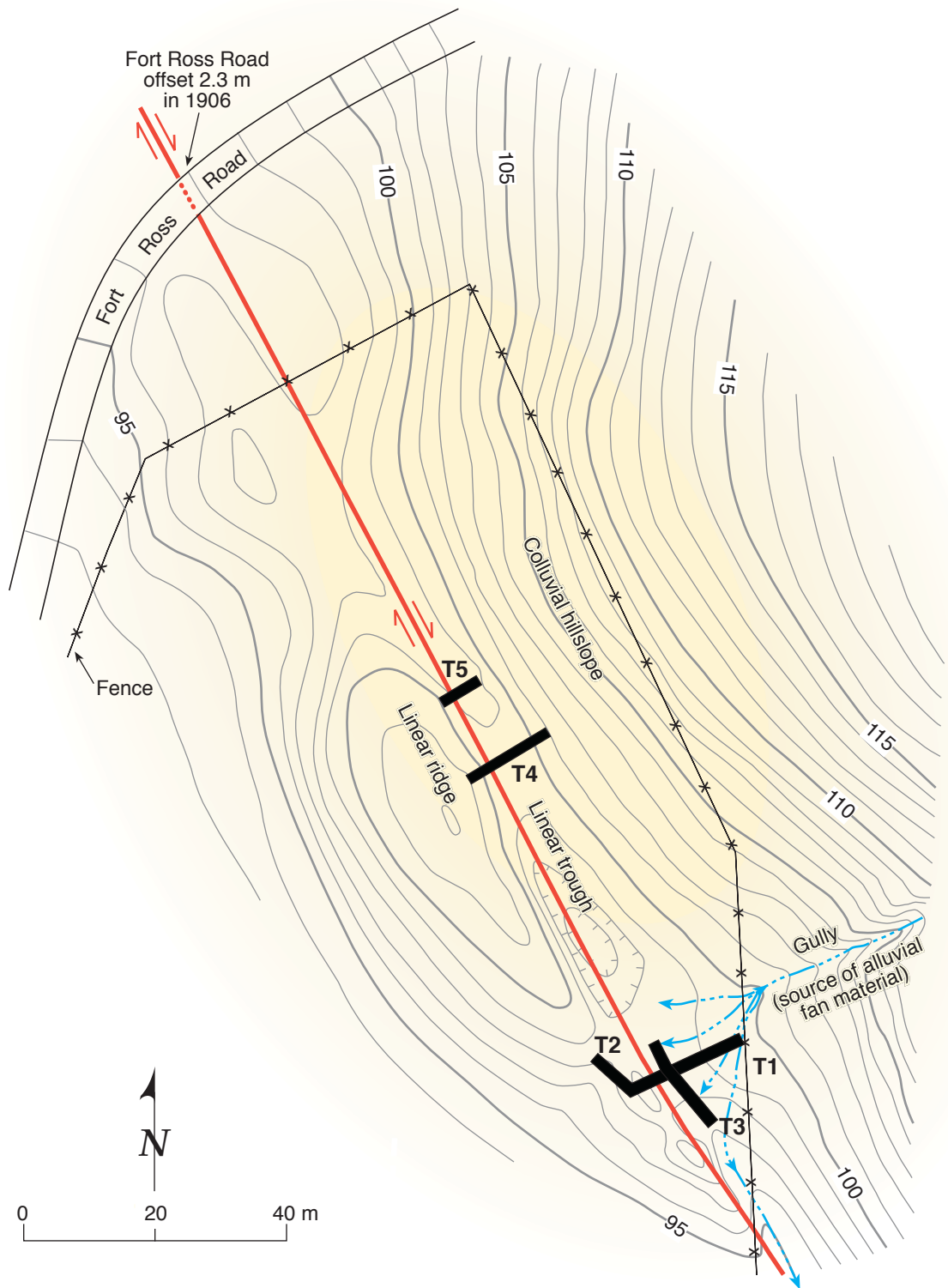


Figure 4. Detailed topographic map of the Fort Ross Orchard site, showing San Andreas fault, and trenches T1 to T5. Contour interval of 1 m uses arbitrary site datum.



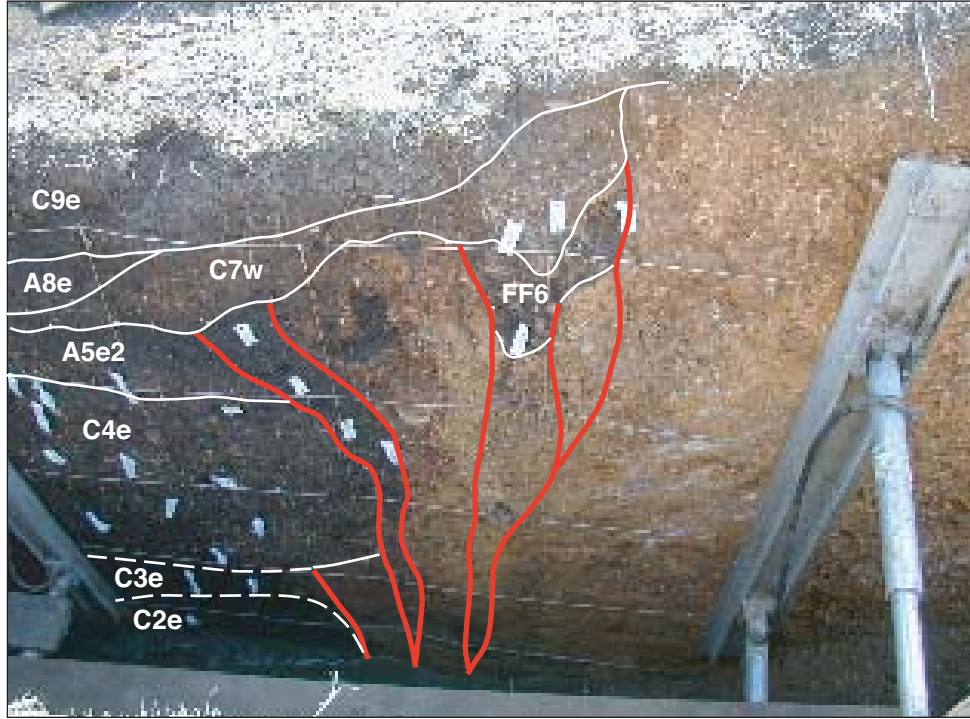
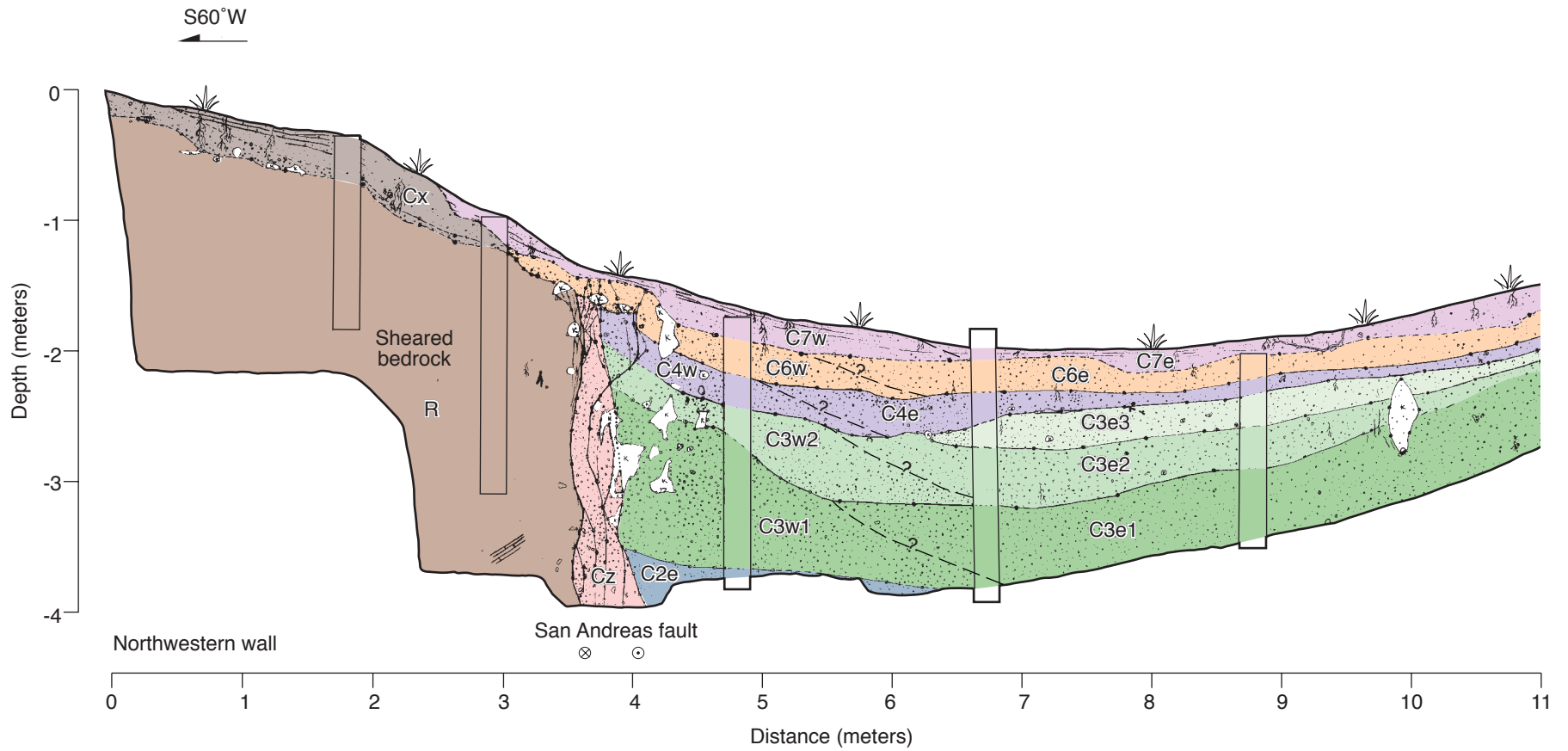


Figure 6. Photograph of San Andreas fault exposed in southeastern wall of Trench 1, showing bedrock on southwestern side of fault, faulted colluvium and alluvium on northeastern side of fault, fissure-fill deposits, and unfaulted colluvium deposited since 1906. White flags indicate locations of charcoal samples, see Figure 5 for unit descriptions.



### Explanation

C7w	C7e	Upper scarp colluvium/hillslope colluvium	Cx	Bedrock residuum
C6w	C6e	Upper middle scarp colluvium/hillslope colluvium	Cz	Sheared colluvium (undifferentiated)
C4w	C4e	Lower middle scarp colluvium/hillslope colluvium	R	Sheared bedrock (Tertiary German Rancho Fm.)
	C3e3	Hillslope colluvium	K	Krotovina (animal burrow)
C3w2	C3e2	Lower scarp colluvium (fine-grained) and hillslope colluvium		
C3w1	C3e1	Lower scarp colluvium (coarse-grained) and hillslope colluvium		
C2e		Hillslope colluvium		

Figure 7. Log of northwestern wall of trench 4, Fort Ross Orchard site.

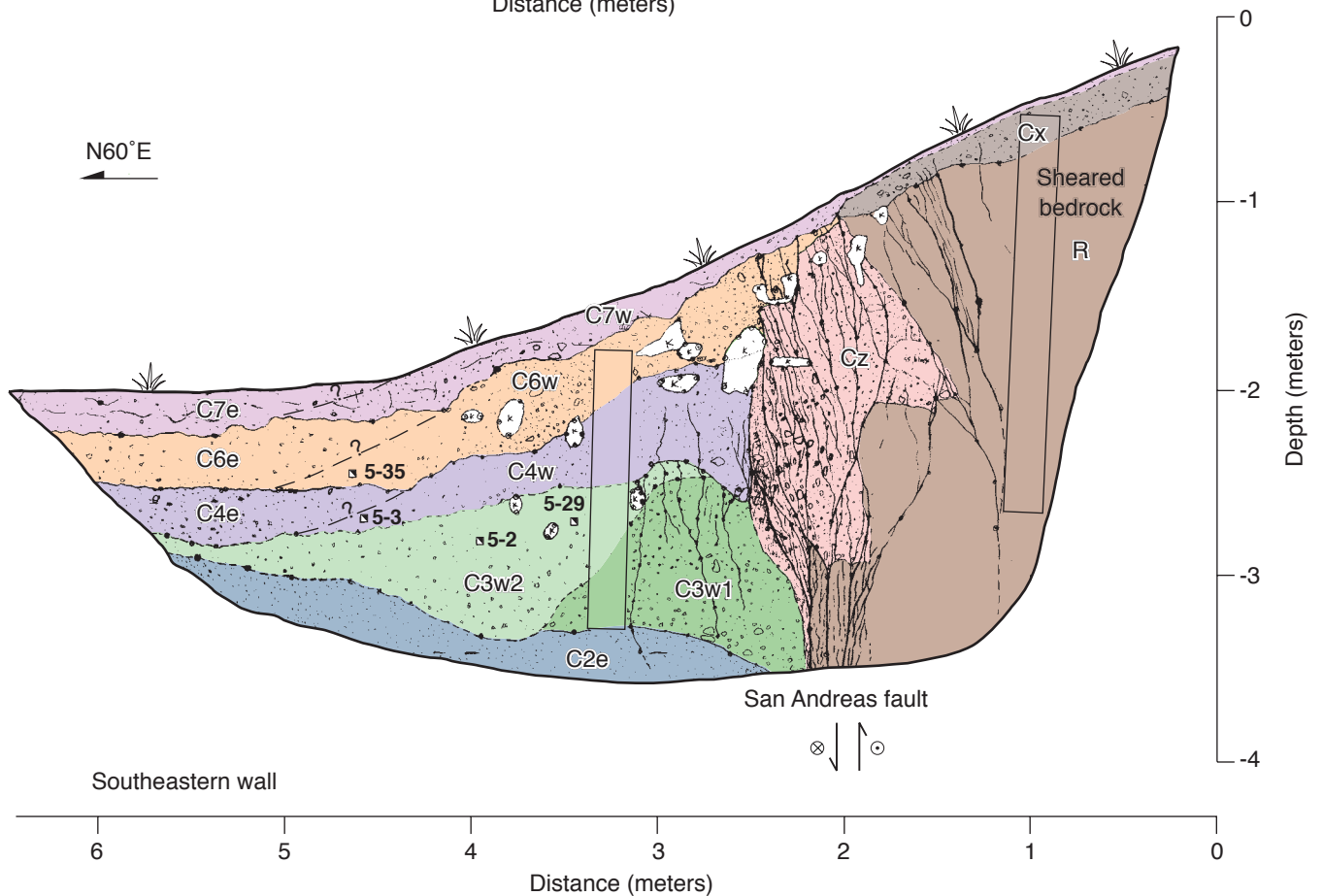
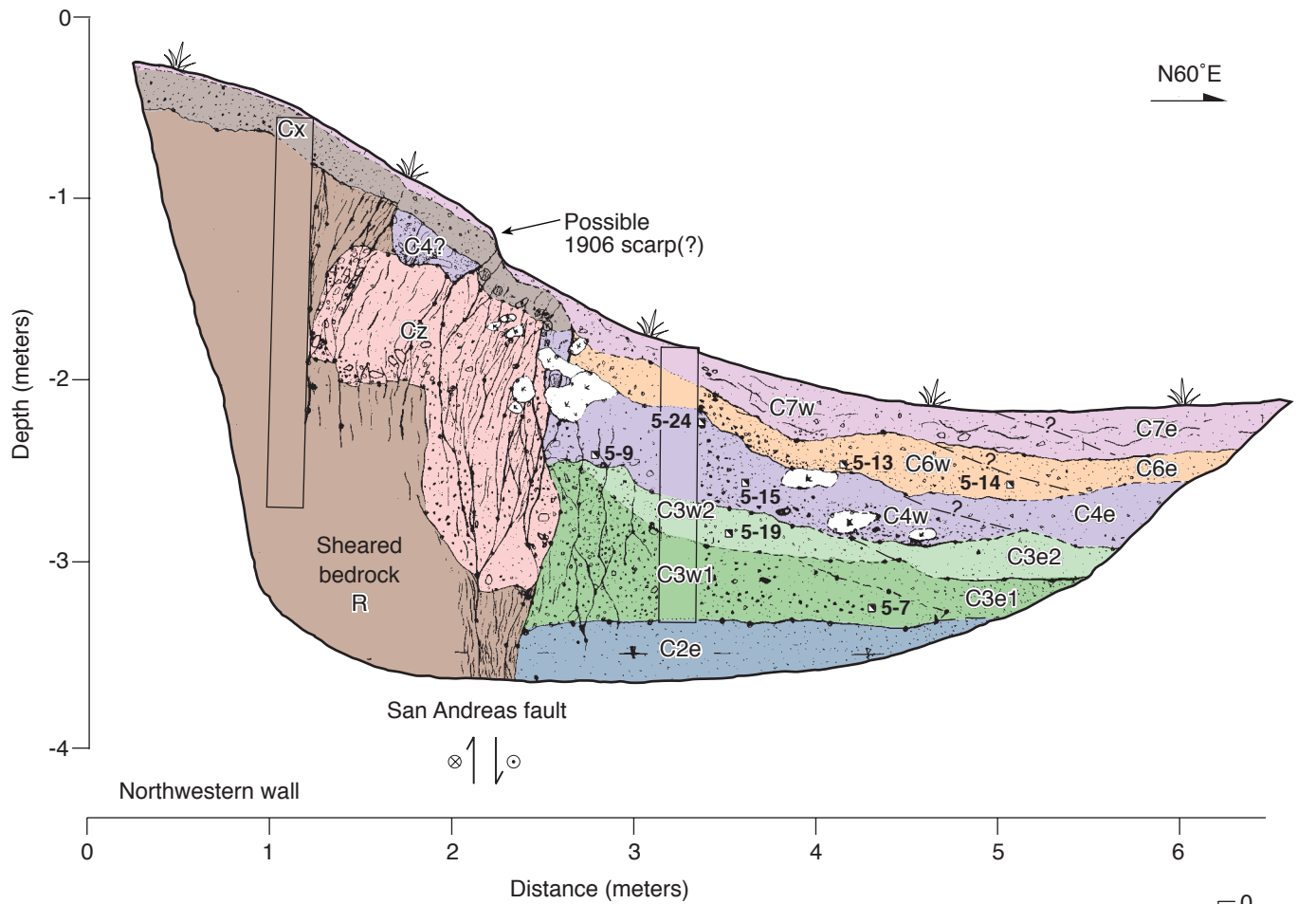


Figure 8. Logs of northwestern and southeastern walls of trench 5, Fort Ross Orchard site. See Figure 7 for generalized unit descriptions.

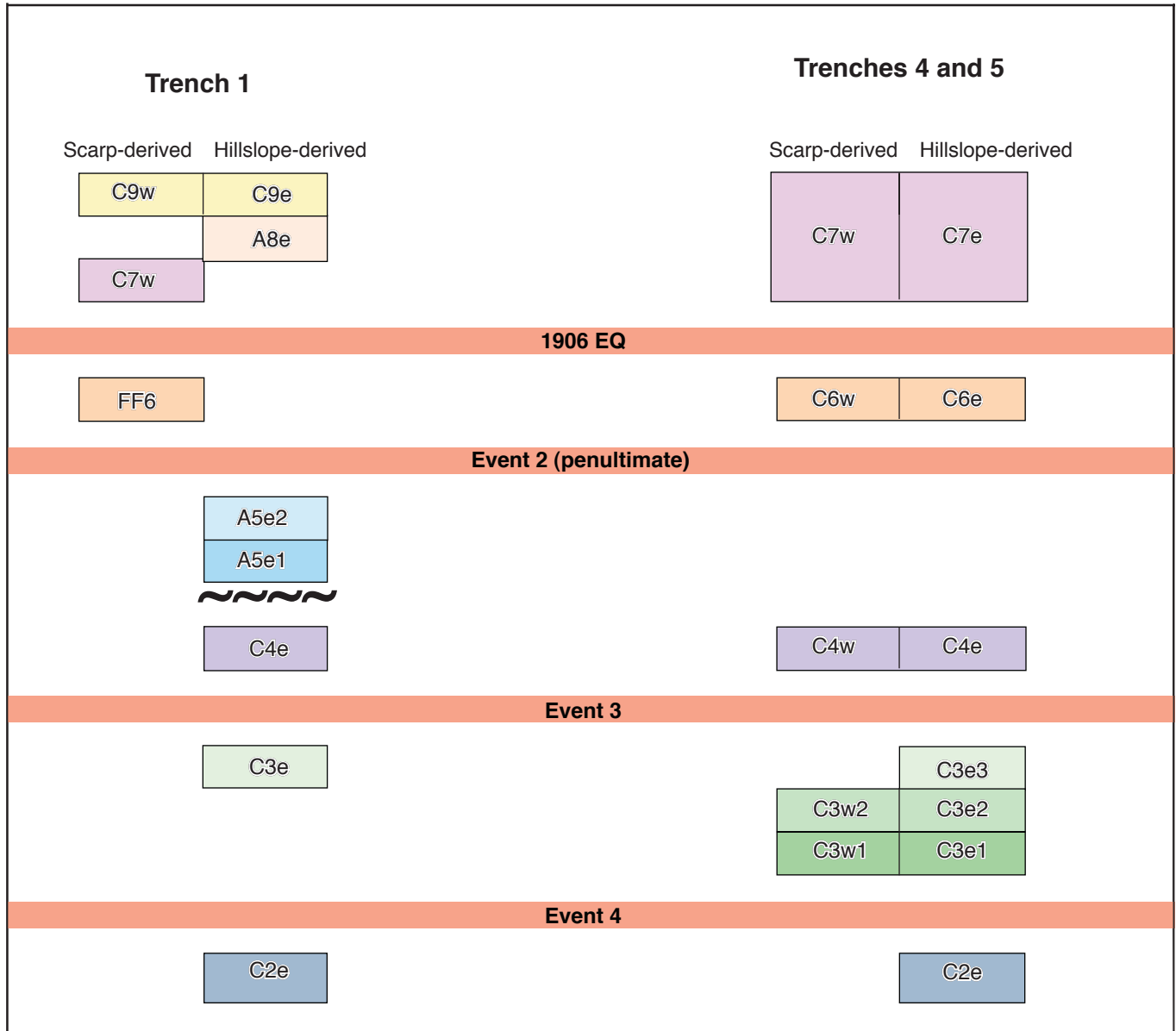


Figure 9. Stratigraphic relationships on the eastern side of the San Andreas fault, Fort Ross Orchard site. Unit designations assigned with C = colluvium, A = alluvium, FF = fissure fill; numbered with younger deposits having higher numbers; and w = derived from western source, and e = derived from eastern source.

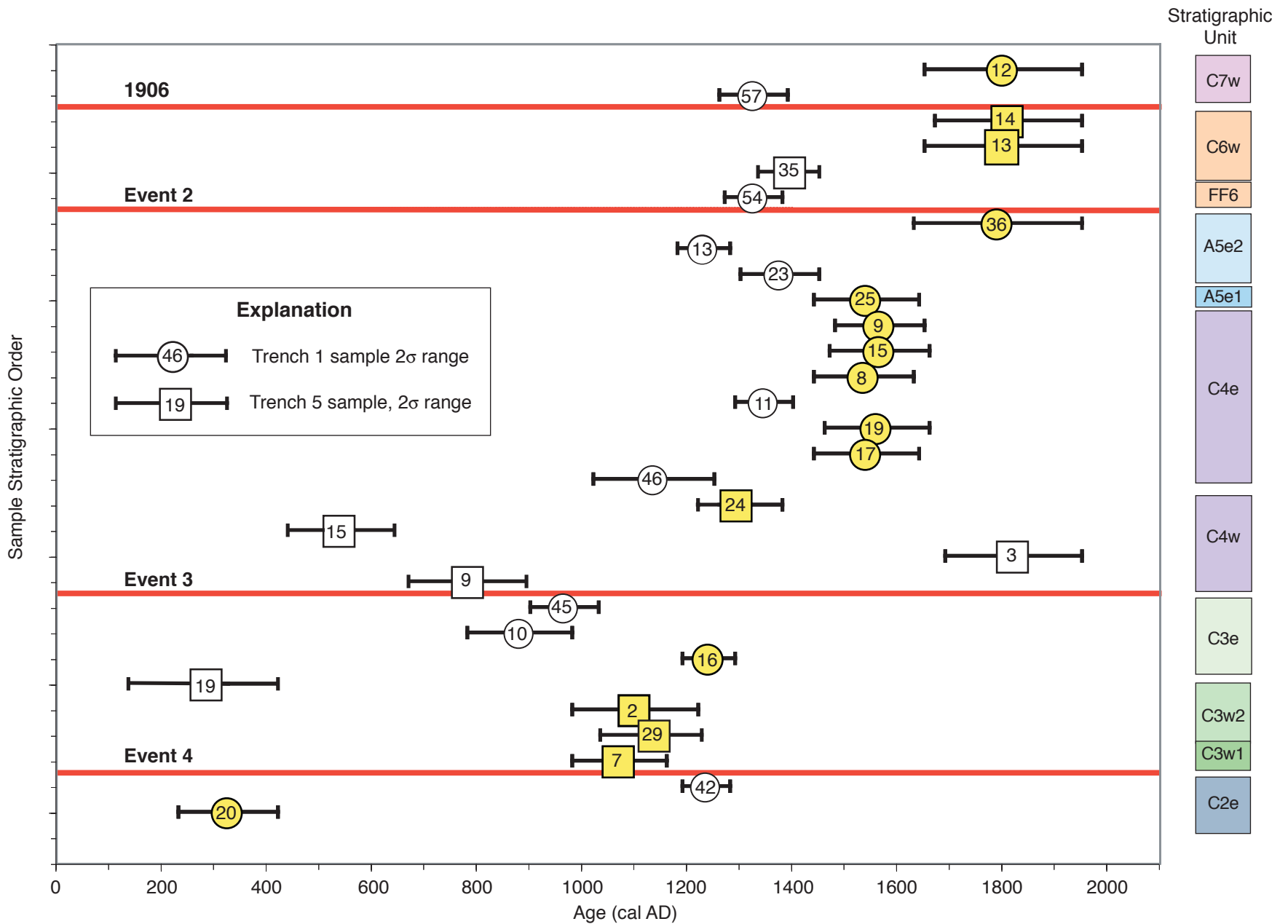


Figure 10. Calibrated 2-sigma radiocarbon ages plotted by relative stratigraphic order. Sample number in circles are from trench 1; sample numbers in squares are from trench 5. Samples highlighted in yellow are those interpreted as most representative of deposit age, and are used in OxCal analysis program.

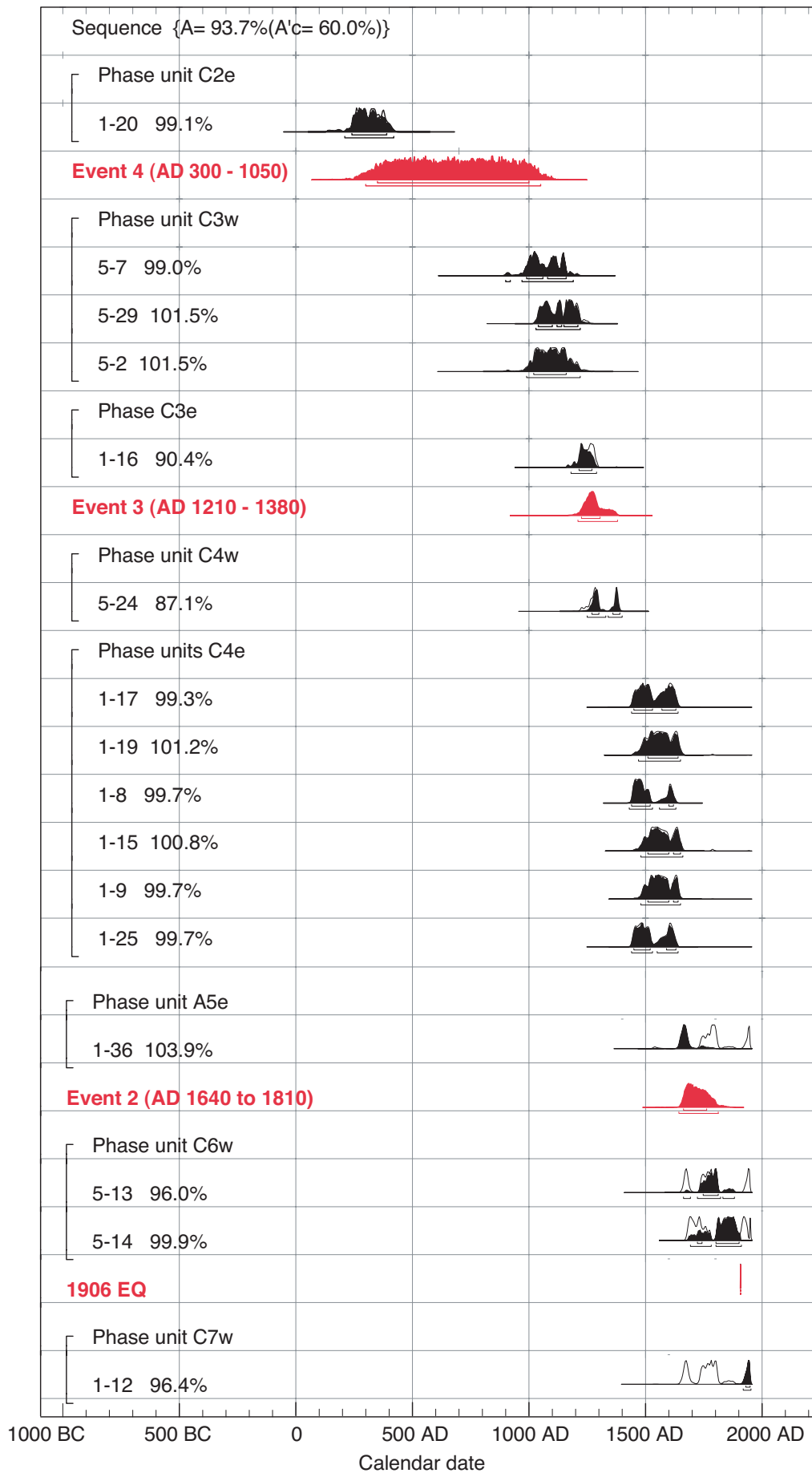


Figure 11. Analytical output from OxCal v 3.9 (Ramsey, 2003), showing radiocarbon sample numbers within each phase, agreement percentages, and probability density functions of each sample and earthquake events.

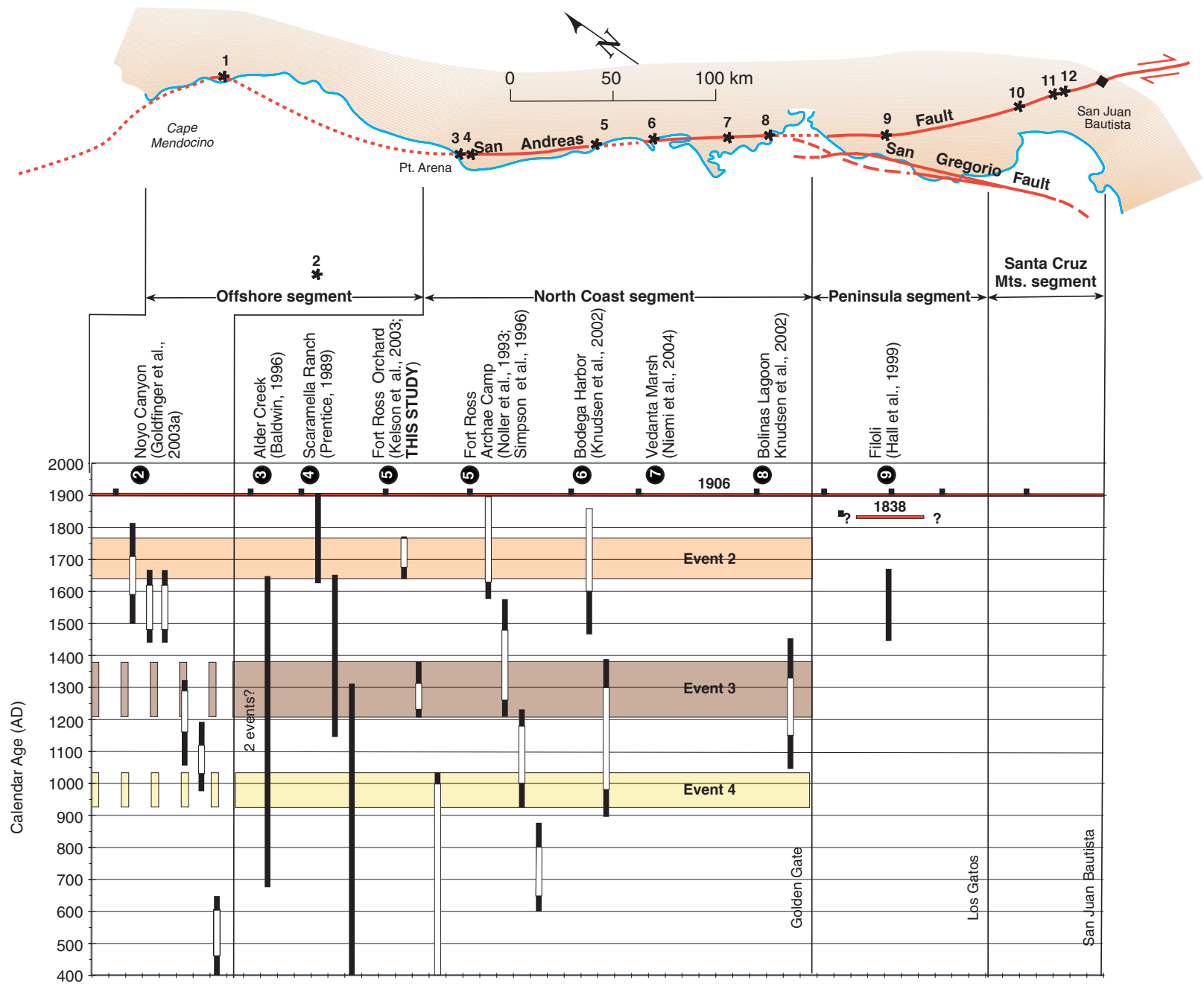


Figure 12. Earthquake chronology along segments of the northern San Andreas fault. Open bars show 1-sigma confidence intervals; solid bars show 2-sigma confidence intervals.